Neurons on tape: Automated Tape Collecting Ultramicrotomy-mediated volume EM for targeting neuropathology

Georg Kislinger[a,b], Cornelia Niemann[a,b], Lucia Rodriguez[a,b], Hanyi Jiang[a,b], Maryam K. Fard[b], Nicolas Snaidero[a,c], Adrian-Minh Schumacher[d,e], Martin Kerschensteiner[f,d,e], Thomas Misgeld[a,b,f], and Martina Schifferer[b,f,*]

[a]*Institute of Neuronal Cell Biology, Technical University Munich, Munich, Germany*

[b]*German Center for Neurodegenerative Diseases (DZNE), Munich, Germany*

[c]*Hertie institute for Clinical Brain Research, Tuebingen University Hospital, Tuebingen, Germany*

[d]*Faculty of Medicine, Biomedical Center (BMC), Ludwig-Maximilians-University Munich, Munich, Germany*

[e]*Institute of Clinical Neuroimmunology, University Hospital, Ludwig-Maximilians-University Munich, Munich, Germany*

[f]*Munich Cluster of Systems Neurology (SyNergy), Munich, Germany*

**Corresponding author: e-mail address: martina.schifferer@dzne.de*

Chapter outline

Methods in Cell Biology, ISSN 0091-679X, https://doi.org/10.1016/bs.mcb.2023.01.012

Abstract

In this chapter, we review Automated Tape Collecting Ultramicrotomy (ATUM), which, among other array tomography methods, substantially simplified large-scale volume electron microscopy (vEM) projects. vEM reveals biological structures at nanometer resolution in three dimensions and resolves ambiguities of two-dimensional representations. However, as the structures of interest—like disease hallmarks emerging from neuropathology—are often rare but the field of view is small, this can easily turn a vEM project into a needle in a haystack problem. One solution for this is correlated light and electron microscopy (CLEM), providing tissue context, dynamic and molecular features before switching to targeted vEM to hone in on the object's ultrastructure. This requires precise coordinate transfer between the two imaging modalities (e.g., by micro computed tomography), especially for block face vEM which relies

on physical destruction of sections. With array tomography methods, serial ultrathin sections are collected into a tissue library, thus allowing storage of precious samples like human biopsies and enabling repetitive imaging at different resolution levels for an SEM-based search strategy. For this, ATUM has been developed to reliably collect serial ultrathin sections via a conveyor belt onto a plastic tape that is later mounted onto silicon wafers for serial scanning EM (SEM). The ATUM-SEM procedure is highly modular and can be divided into sample preparation, serial ultramicrotomy onto tape, mounting, serial image acquisition—after which the acquired image stacks can be used for analysis. Here, we describe the steps of this workflow and how ATUM-SEM enables targeting and high resolution imaging of specific structures. ATUM-SEM is widely applicable. To illustrate this, we exemplify the approach by reconstructions of focal pathology in an Alzheimer mouse model and CLEM of a specific cortical synapse.

1 Introduction

One of the challenges of volume electron microscopy (vEM) lies in the necessity of making tissue accessible to the electron beam for signal detection. In contrast to methods building on other electromagnetic radiation, including light microscopy or X-ray based techniques, electrons do not penetrate thicker biological samples in a manner that would allow image formation (Morales et al., 2016; Parlanti et al., 2017; Rawson et al., 2020). Consequently, vEM methods to analyze all but the thinnest cellular structures typically require tissue sectioning (Gay & Anderson, 1954). Even transmission EM (TEM) tomography, while providing high axial resolution and seamless reconstructions, can do so only in a limited thickness of 500 nm, the typical diameter of a large organelle, such as a mitochondrion (De Rosier & Klug, 1968; Yan, Voorhees, & Xin, 2020). Ultrathin sectioning ($<$100 nm) enables full accessibility to the electron beam and is either accomplished using a diamond knife on an ultramicrotome or by ion or gas beams scanned over the sample (block) surface. Knife-based techniques for vEM can be subdivided into block face and section collection (array tomography) approaches (Peddie et al., 2022). In the former, the block surface is documented by scanning electron microscopy (SEM), and then removed by an ultramicrotome that is integrated into the vacuum chamber of the EM, after which the process is repeated (serial block face, SBF-SEM) (Denk & Horstmann, 2004). This has the advantage of generating well-aligned stacks of largely undistorted sections. In contrast, collecting serial sections on durable supports (Collman et al., 2015; Kasthuri et al., 2015; Schalek et al., 2012; White et al., 1986) is modular with separated ultramicrotomy and imaging steps. Consequently, SEM imaging of sections—instead of block faces—diminishes charging and renders the tissue accessible to postembedding labeling and multiscale imaging. The resulting storable “tissue libraries” can be repeatedly imaged with adjusted conditions such as resolution or contrast. This storage and re-inspection option is especially attractive in the context of precious samples fixed for EM (e.g., from human pathology).

Historically, serial sectioning on TEM slot grids was a tedious procedure that required substantial amount of training—and even the most skilled practitioners were limited by the slot geometry (2 mm) and the stability of the thin films that support the sections (Bang & Bang, 1957; Harris et al., 2006; White et al., 1986). This restriction and the lack of available automation options has given rise to the development of "array tomography" (AT) approaches (Collman et al., 2015; Wacker & Schroeder, 2013), collection-based volume SEM techniques. While losing TEM resolution, AT allows the usage of larger and more durable support structures in order to collect and—even repetitively—inspect the sample of interest within its larger anatomical context. One robust and largely automated sectioning and collection system was developed by Jeff Lichtman's laboratory and is known as "*A*utomated *T*ape-collecting *U*ltra*m*icrotomy" (ATUM) (Kasthuri et al., 2015; Schalek et al., 2012). This technique relies on serial sectioning of tissue on a standard ultramicrotome, which is retrofitted with a conveyor belt made of flexible conductive plastic, onto which sections are collected in order from the diamond knife's water bath (Baena et al., 2019). Sections are not necessarily collected as ribbons, thus allowing greater freedom in sample shape and size (Shibata et al., 2019). These resulting plastic tape strips with sections are cut and mounted on silicon wafers of 10 cm diameter after which the sections are mapped at low resolution (Hayworth et al., 2014) and then serially imaged by backscattered or secondary electron detection in a single (Kasthuri et al., 2015; Morgan et al., 2016) or multibeam SEM (Eberle & Zeidler, 2018; Shapson-Coe et al., 2021). The resulting images are registered and the objects of interest segmented and reconstructed, similar to other vEM approaches (Berger, Sebastian Seung, & Lichtman, 2018; Kornfeld & Denk, 2018).

While originally developed for "connectomics" reconstructions of neuronal connectivity at large scales (Kasthuri et al., 2015; Morgan et al., 2016; Shapson-Coe et al., 2021), the massive acceleration of the serial sectioning process in ATUM also enables routine studies of cell biology or subcellular pathology, where three-dimensional representations of ultrastructure are needed to unambiguously reveal intracellular geometry or complex cellular contacts. For instance, using this method applied to cell biology, the "parking garage" model of ER stacks (Terasaki et al., 2013), cell–cell contacts in ovarian follicles (Baena & Terasaki, 2019; Norris & Terasaki, 2021) and kidney glomerulus architecture (Terasaki, Brunson, & Sardi, 2020) were described. Examples in neurobiology—including our own work—are the unusual pattern of cortical myelination (Tomassy et al., 2014), presynaptic mitochondria (Thomas et al., 2019), the characterization of neurovascular contacts in cortex (Mondo et al., 2020), myelin pathology (Djannatian et al., 2019), or dysmorphic axons after astrocyte injury (Herwerth et al., 2022).

Beyond enabling the collection of large series of ultrathin sections, the modular nature of ATUM (and related AT approaches; (Burel et al., 2018; Collman et al., 2015; Micheva & Phend, 2018; Templier, 2019; Wacker & Schroeder, 2013)) is advantageous in applications where specific or simply rare objects need to be found in a large tissue block (Wacker et al., 2018). While in such a setting, the final volume to be analyzed at full resolution might be small, the ability to scan large areas at low

resolution, followed by hierarchical imaging of decreasing fields of view and increasing resolution to hone in on the object of interest allows search strategies that are not feasible with other approaches (Schifferer et al., 2021). This targeted imaging approach is especially suitable for correlative light and electron microscopy (CLEM) studies, aiming at the vEM visualization of the same structure that was previously observed by light microscopy (Fang et al., 2018; Hirabayashi, Tapia, & Polleux, 2018; Kamasawa et al., 2015; Snaidero et al., 2020; Sun et al., 2020). Similarly, precious tissue and cell samples, e.g., from patients (Liesche-Starnecker et al., 2022; Shapson-Coe et al., 2021), can be preserved as section libraries and repeatedly queried for rare instances of pathological change based on the "unbiased" tissue contrast that standard heavy-metal staining of EM samples provides similar to other histological stains. Given these advantages and the fact that ATUM thus far is not widely used outside of the "connectomics" applications for which it was devised, we provide here an overview of the technique and a number of variations that we find especially useful for hierarchical imaging of correlated and/or pathological samples, hoping to make the technique accessible to more users.

2 Rationale

AT and especially ATUM techniques, despite several advantages as mentioned before, are still not used frequently compared to other vEM methods, especially in EM core facilities. RMC Boeckeler provides the only commercial solution based on the prototype from Jeff Lichtman's group, with the ATUM collector connected to and controlled by an ultramicrotome (PowerTome, RMC Boeckeler). Recently, an alternative academic system called "AutoCUTS" with a collector fitted onto a UC6 ultramicrotome (Leica) was developed (Li et al., 2017). Focused ion beam (FIB) and serial blockface (SBF) SEM might seem more approachable, as they are fully commercialized, and are considered more robust. The underrepresentation of ATUM among the vEM family is also reflected by the number of hits in a simple PubMed search for "FIB-SEM" (677), "Serial Block Face SEM" (418) vs "Array Tomography" (293) and "ATUM" or "Automated Tape Collecting Ultramicrotomy" (65) since 2005. Therefore, with providing this Chapter, we want to lower the barrier of entry for using ATUM and assist in fully exploiting the potential of existing workflows built around this powerful approach.

The different chapters of the methods section represent the actual steps of the modular ATUM workflow (Fig. 1). We start with comments on standard *en bloc* embedding for vibratome sections from mouse cerebral cortex as an example (2.1). We build on key sample preparation protocols (Deerinck et al., 2010; Hua, Laserstein, & Helmstaedter, 2015; Tapia et al., 2012) and only highlight aspects that are particularly important for the ATUM workflow. Serial sectioning requires sample block trimming (2.2) and the preparing of plastic tape (2.3). The actual serial sectioning, collection and mounting is described in detail (2.4). After collection, the

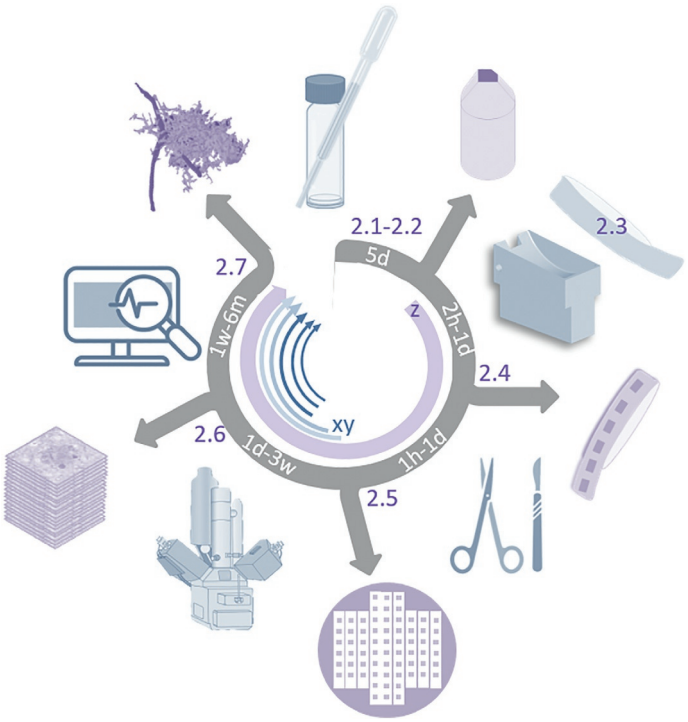

FIG. 1

Workflow overview. Schematics of all steps in the workflow as described in this chapter in different paragraphs (indicated as numbers, blue icons): sample preparation (2.1) and trimming (2.2), ultramicrotomy (2.4) with prepared plastic tape (2.3), wafer mounting (2.5), image acquisition (2.6), image analysis (2.7). The outputs at each step are illustrated in violet (clockwise: trimmed block, sections on tape, assembled wafer, image series, three-dimensional model). The timing of each step is indicated (white numbers). The inner circle illustrates the determination of axial (violet, z) and lateral (blue, xy) resolution. The axial resolution is determined at the ultramicrotomy step. These are important decision points for the operator. In contrast, the lateral resolution (and field of view) can be flexibly adjusted as serial section collection preserves reimaging and hierarchical imaging options.

sample is mounted onto a wafer and optionally pre-cleaned in a vacuum chamber (2.5). We delineate the actual imaging procedure on two widely used SEM systems (Zeiss Crossbeam 340, Thermo Apreo S2), including distinct software types (Atlas 5, Maps 3, respectively) as these systems are available in our lab, diverge and may provide a better insight in challenges and opportunities (2.6). We illustrate a typical image registration and manual segmentation process using the software packages Fiji TrakEM2 (Schindelin et al., 2012), VAST (Berger et al., 2018) and Blender (Brito, 2018) (2.7).

3 Methods

3.1 Tissue preparation

Timing: 5d.

3.1.1 Principle

In general, sample preparation for ATUM is very versatile and can be applied to existing samples that were initially prepared for other volume SEM techniques or TEM. All tissue blocks that can be sectioned at the desired thickness and allow SEM imaging with secondary electron (SE) or backscattered electron detection (BSD). If sample blocks are specifically dedicated to ATUM-SEM, there are, however, a few considerations that can facilitate downstream processing. For instance, the choice of contrasting and infiltration protocols influences both, cutting performance and image formation.

In order to generate homogenous contrast, *en bloc* staining is recommended for standard samples of up to 500 µm edge length. We are often dealing with brain vibratome sections, prepared at ~1.5–3 mm lateral edge length and ranging from 30 to 500 µm thickness. For tissue sections below 100 µm thickness we apply the "Ellisman/Tapia rOTO protocol" (Deerinck et al., 2010; Kislinger et al., 2020a; Tapia et al., 2012) with a reduced osmium step, TCH and another osmium step. For thicker samples, the "Hua rOTO protocol" with separated osmium and potassium ferrocyanide steps is applied as it facilitates heavy metal penetration (Hua et al., 2015). We omit the lead aspartate step as we see that it is not needed for image formation and can cause staining gradients. BROPA, fBROPA and other larger scale staining methods for even bigger tissue cubes comprising more than 1 mm edge length are potentially suitable as well (Genoud et al., 2018; Mikula & Denk, 2015). In case of problematic tissue with limited stain penetration or sample blocks originally prepared for TEM (rO protocol), post-contrasting after sectioning and mounting can be performed to increase contrast (see Section 3.3) (Hayworth et al., 2015; Morgan et al., 2016). Tissues or cells with any additional treatment like immunogold (Mikuni et al., 2016; Norris & Terasaki, 2021; Sun et al., 2020) or APEX staining (Thomas et al., 2019) can be assessed by ATUM sectioning and imaging. However, the overall stain load should be limited in favor of decent microtomy properties. In general, epoxy resins are preferred over methacrylate due to superior cutting and imaging characteristics. Indeed, while other AT techniques are mostly based on methacrylate resins (LR White/Gold or Lowicryl) (Micheva & Smith, 2007), there is, so far, only one publication on ATUM of Lowicryl embedded samples (Norris & Terasaki, 2021).

A major challenge for serial sectioning and collection is the occurrence of section folds (see Section 7, Fig. 11). One of the reasons for the occurrence of sectioning folds are differences in the cutting properties of tissue vs empty resin. This problem increases with stain load, e.g., at white matter areas with highly contrasted myelin compared to gray matter regions. While large scale folds can be seen at regional

tissue and tissue-resin borders (Fig. 11A), smaller folds can arise locally in case of tissue staining heterogeneity, e.g., at blood vessel lumen vs endothelium (Fig. 11C). In order to overcome large scale folds, the sample can be embedded into surrounding support tissue which ideally has similar characteristics (Hildebrand et al., 2017). While a thorough comparison is pending, the epon-araldite resin LX112 has been proven to reduce miniature folds that occur due to density differences in the interface between tissue and resin (Wanner & Vishwanathan, 2018).

If ATUM is performed on a vibratome tissue section and a specific region is targeted, e.g., in a correlative workflow, it is very important to keep the tissue as flat as possible. Vibratome sections tend to wrinkle up during heavy metal infiltration, a problem that increases with thinner and larger sections. In CLEM experiments, this deformation hampers the alignment of the confocal imaging plane with the ultramicrotome sectioning plane. The easiest way to flatten tissue during embedding is to minimize heavy metal load and restrict dissection of the region of interest to a minimal size ($<1 \times 1$ mm). Vibratome sections can also be adhered to glass slides using a proteinous "glue" or sandwiched between filters (Luckner & Wanner, 2018) to splint the section.

3.1.2 Materials

3.1.2.1 Equipment

- dissecting knife
- fine brush
- binocular
- glass vials
- orbital shaker
- Parafilm
- gelatin capsules
- OPTIONAL: laboratory microwave with cooling option and vacuum chamber
- OPTIONAL: ultrasonic bath

3.1.2.2 Reagents

- 0.1 M cacodylate buffer pH 7.4
- paraformaldehyde
- glutaraldehyde
- calcium chloride
- osmium tetroxide crystalline
- thiocarbohydrazide
- potassium ferrocyanide
- uranyl acetate
- ethanol
- acetone
- resin components LX112
- LX112 resin (glycid ether, DDSA, NMA, DMP-30)

3.1.3 Step-by-step protocol

SAFETY: Most reagents are toxic and/or cancerogenic. Protective equipment and handling under a suitable chemical fume hood is mandatory.

NOTE: All steps are handled in glass vials (Fig. 2B). EM-grade reagents and deionized water are used. All reagent exchange and washing steps (Fig. 2C) are performed with as much volume as possible. The tissue must not get dry at any point but reagents are added immediately. The washing is first done twice, then with incubation steps in between. The microwave protocol is recommended for better penetration, especially for bigger samples, at the infiltration step. All incubation steps are performed in a laboratory microwave with vacuum function except for acetone incubation and infiltration with resin concentration higher than 75% (BioWave, PELCO) (Fig. 2C). After the microwave procedure, the glass vials with the samples are positioned onto an orbital shaker (Fig. 2C) under the fume hood.

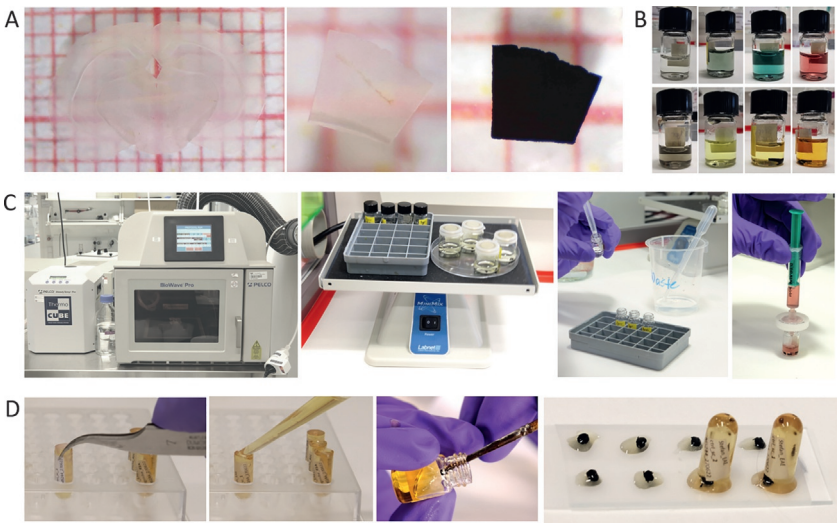

FIG. 2

Embedding procedure. (A) Stereomicroscopic images showing brain tissue sections on scale paper. A coronal, 50 μm thick brain section (left) was dissected to yield a $\sim 1 \times 1 \times 0.05$ mm piece of tissue (middle) that was in turn osmicated (right). (B) Photographs of the tissue sample in a glass vial at different embedding steps (from left to right): buffer, osmium, potassium ferrocyanide, TCH, osmium, uranyl acetate, 25% resin, 100% resin. (C) Photographs of (from left to right) the microwave with cooling unit, orbital shaker with samples, sample wrack, filtering (D) Photographs of sample embedding (left to right): positioning of the label into the gelatin capsule, resin filling of gelatin capsule, tissue removal from glass vial with brush, tissue positioning on glass slide with Parafilm and capsule inversion onto it.

1. The mouse is perfused by quickly flushing with one blood volume of 0.1 M cacodylate buffer and then immediately afterwards using 4% paraformaldehyde, 2.5% glutaraldehyde and 2 mM calcium chloride in 0.1 M cacodylate buffer pH 7.4. The speed is set to ~1.3 mL/min. The fixative is prepared freshly (<2 h before perfusion). Opened ampoules are not reused
2. The brain is dissected and fixed in the same fixative over night at 4 °C
3. Vibratome sectioning at 50–200 µm thickness is performed in PBS and the sections are postfixed over night at 4 °C
4. Sections are washed in 0.1 M cacodylate buffer three times 10 min and stored at 4 °C until further processing (Fig. 2A)

   Pause point: The fixed samples can be stored several days or weeks in the fridge. Note that membrane and lipid fixation is not completed and requires osmification.
5. The vibratome brain section is dissected under a binocular using a microdissection knife according to light microscopy images or to other anatomical information regarding the localization of the ROI (Fig. 2A)
6. The tissue is transferred to a glass vial with 0.1 M cacodylate buffer using a fine brush (Fig. 2B)
7. The section is washed three times 10 min with 0.1 M cacodylate buffer
8. Postfixation is done in (reduced: add 2.5% potassium ferrocyanide = "Ellisman protocol"; non-reduced: no additive = "Hua protocol") 1% osmium tetroxide in 0.1 M cacodylate buffer pH 7.4. Osmium crystals are brought into solution by using liquid nitrogen and/or in an ultrasonic bath (15–20 min). Special caution should be taken as osmium crystals are particularly toxic. Incubate for 1 h at RT
9. OPTIONAL ("Hua protocol" (Hua et al., 2015)): if non-reduced osmium is applied, it is replaced by filtered 2.5% potassium ferrocyanide in 0.1 M cacodylate buffer without any additional washing step. However, it is advisable to remove as much osmium as possible. With residual osmium the liquid turns brown, with almost no osmium the color turns transparent blue (Fig. 2B)
10. Wash the tissue three times 10 min with 0.1 M cacodylate buffer
11. Exchange for filtered (0.2 µm membrane filter) 1% aqueous TCH (stirred for 20 min at 60 °C until it is transparent or slightly pink or brown) and incubate for 25 min at 40 °C (Fig. 2C)
12. Wash three times with water
13. Apply 1% aqueous osmium tetroxide for 1 h
14. Wash three times with water
15. The section is transferred into a new glass vial using a brush. This avoids floes of residual heavy metal contamination and enables the incubation in a smaller volume of expensive and radioactive uranyl acetate
16. Stain with 1% uranyl acetate and incubate at 4 °C overnight and 2 h at 50 °C. Protect the sample and the reagent from light in order to prevent precipitation

    SAFETY: Be careful, uranyl acetate is radioactive.

17. Dehydrate sample with a graded ethanol series (15%, 30% 40%, 50%, 60%, 70%, 80%, 90%, 100%, 100%, 100% ethanol), increasing the ethanol concentration every 10 min
18. Change from 100% ethanol into 100% acetone and exchange twice, 15 min each
19. Prepare the resin by mixing 10 g of LX112 with 6.45 g of DDSA and 4.35 g of NMA and stir for 10 min. Add 0.3 mL DMP-30 and stir for 20 min. Start infiltration in resin in acetone (25%, 50%, 75%, 90%) for 2 h each and 100% resin overnight. Change to fresh resin the next day and incubate for 4 h
20. Transfer the tissue onto Parafilm-coated glass slides. Fill a gelatin capsule with resin and invert it onto the tissue piece (Fig. 2D)
21. Cure resin blocks at 60 °C for 48 h in an oven

PAUSE POINT: The cured sample blocks can be stored for years.

3.2 Trimming

Timing: 1–2 h.

3.2.1 Principle

Similar to any other ultramicrotomy experiment, sample blocks are tightened and positioned deep into the holder to avoid section thickness variations which appears as stripes of different colors on the section (Fig. 3A and F). Sample block trimming determines key parameters including block face size and geometry, which impact the ease and mode of sectioning and collection (Baena et al., 2019). Trimming of the block face at tilt angles larger than 5° has to be avoided as the angle of the tape collector is fixed and cannot be adjusted accordingly. If the sample is not flat, it is recommended to compensate this by a sample holder tilt (top to bottom, not left to right) (Fig. 3C and E). Usually, block faces of 0.8–2.5 mm edge length are selected for single section pick-up whereas smaller sections are rather collected as short ribbons (3–10 sections). For single section collection, a rectangular shape with the shorter edge being the cutting edge reduces compression. In addition, a longer lateral edge prevents turning or loss of sections before collection. In contrast, a longer trailing edge increases section density on the tape and reduces the number of wafers needed for a given amount of sections. We prefer cutting off one corner to generate an asymmetric section providing a directional tag for all subsequent steps. Ribbons can be generated from similarly shaped block faces or from trapezoid sections with a longer leading than trailing edge as this reduces the tension between the sections and eases the separation of ribbon series of 3–10 sections from each other (Fig. 3). The knife angle should be set to 0° as the tape collector cannot be tilted and is ideally positioned parallel to the knife edge (Fig. 3F). The block face ideally only contains tissue and no empty resin as any transition from tissue to resin can result in fold formation. Therefore, it is recommended to trim away most of the redundant tissue (Fig. 3). Blocks are trimmed either as a pyramid using a trimming machine (TRIM2, Leica) at a 40–60° angle or by a

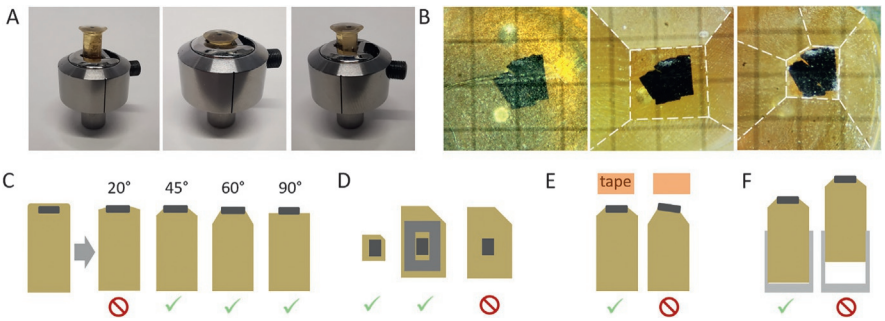

FIG. 3

Optimized trimming of resin blocks. (A) Photos of sample block positioned to far outside (left), too far inside (middle) and correctly (right) in the sample holder (B) Ocular photos of the untrimmed (left), trimmed with too much surrounding resin (middle), correctly trimmed (right) tissue block. (C–G) Schematics of resin block at side (C, E, F) and top (D, G) views. Red-labeled illustrations indicate non-optimal, green ticks preferred positioning. (C) Suitable pyramid angles generated by diamond knives or in a trimming machine range from 45° to 90°. (D) Ideally, the tissue vs empty resin content is increased, if needed with additional support tissue (middle, lighter gray). (E) The block face should be trimmed at 0° in order to be flexible regarding the orientation in the microtomy. The tape collector nose tilt angle is fixed and cannot be adjusted. (F) The block has to be fixed well into the holder with only maximally 50% of its length sticking out to avoid vibrations.

trimming diamond knife generating 60 or 90° angles, respectively (TRIM90, Diatome). While a 90° angle results in equally sized sections independent of sectioning depth, pyramid block sections increase in size with sectioning depth. In our hands, this size differences are not problematic for section mapping during acquisition in small-scale projects (<2000 sections). Furthermore, diamond knife trimming is prone to errors: If the edge generated by trimming is not completely smooth but shows protrusions, these can cause the generation of resin crumbs during sectioning. These small resin particles can then accumulate at the knife edge which interferes with sectioning and/or section separation. To minimize this problem and generate a homogenous trimming edge, the section thickness should be set to <300 nm at a speed of max. 2 mm/s during trimming.

3.2.2 Materials

3.2.2.1 Equipment

- sample holder
- OPTIONAL: diamond trimming knife TRIM90 (Diatome)
- OPTIONAL: TRIM2 trimming machine (Leica)

3.2.3 Step-by-step protocol

(1) Position the block into a sample holder. Make sure to fix it properly with maximally one third of the block protruding from the holder (Fig. 3A and F). Loose clamping can lead to striation and other disturbances during sectioning

(2a) Trim a pyramid at a 45–60° angle using a trimming machine (Fig. 3C). The block face should contain mostly tissue and have an edge length of 0.5–2 mm (Fig. 3B and D).

(2b) ALTERNATIVE: Trim at a 60 or 90° angle using a diamond knife trimming tool (TRIM60, TRIM90) on an ultramicrotome. The Powertome or any other microtomy software can be used for trimming. The maximal speed is set to 2 mm/s and the section thickness to not >300 nm. It is recommended to choose a trimming depth that is 150–200% of the actual target sectioning depth. As the maximal feed of the microtome is 200 µm it has to be reset for two or several trimming rounds. Restore the alignment after resetting the microtome as any inaccuracy will lead to unevenness or edges which, in turn, can interfere with sectioning

(3) Use a deduster to remove resin fluffs that could disturb serial sectioning

PAUSE POINT: Trimmed blocks can be sectioned on another day but the block face might not be flat. If regions at the very surface are of interest, trimming on the same day is recommended.

3.3 Tape preparation

Timing: 1–2 h.

3.3.1 Principle

Tape quality is of great importance for collection, mounting and the choice of image detection. The standard ATUM tape is 8 mm in width, 15–50 m long and is stored on a reel. Conductive tape enables both, SE and BSD detection while samples on non-conductive tape have to be carbon-coated after wafer assembly and, due to the carbon layer on top of the tissue section, only allow BSD detection (Fig. 4A). Two different kinds of conductive tape, carbon-coated Kapton (ccKapton) and carbon nanotube (CNT) tape (Kubota et al., 2018; Schalek et al., 2012) have been applied for ATUM-SEM (Fig. 4). CcKapton is preferred over CNT tape regarding section visibility, especially for ultrathin sections (Fig. 4B). This is important to avoid cutting through tissue sections during the generation of tape strips for wafer assembly (see Section 3.5.1). In addition, the signal-to-noise ratio for acquisition by BSD detection is better on ccKapton compared to CNT tape (Fig. 4C).

It is highly recommended to plasma discharge tape before section collection in order to reduce hydrophobicity and hence prevent wrinkle formation. We use a custom-built plasma treatment instrument for tape reels based on a standard instrument (easiGlow, PELCO) according to the idea and plans proposed by Jeff Lichtman's (Schalek et al., 2012) and Mark Terasaki's (Baena et al., 2019) groups with slight modifications (Fig. 5A). Usually, tape has to be plasma-treated maximally 1 month before ATUM sectioning but optimally freshly right before collection. However, several treatment rounds possibly reduce conductivity. In order to check for tape hydrophilicity, a water drop can be positioned on the tape in order

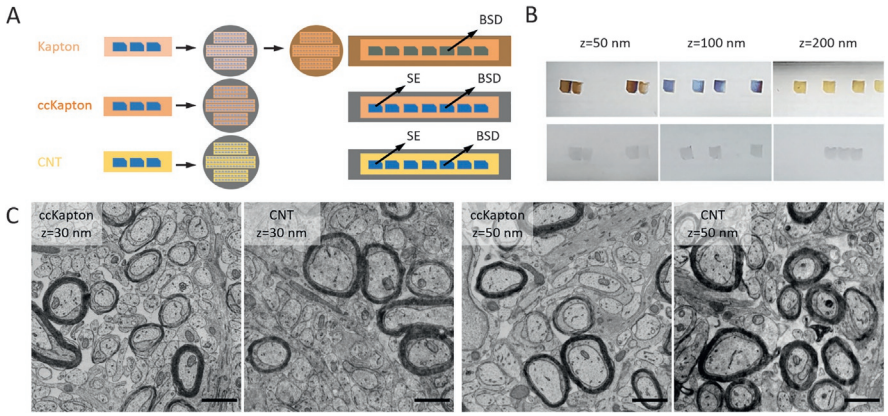

FIG. 4

Tape options. (A) Characteristics of different tapes: Kapton, carbon conductive Kapton (ccKapton) and carbon nanotube tape (CNT). Wafer with non-conductive Kapton can be carbon-coated after assembly (right wafer, orange cover) but are only accessible to BSD, not to SE detection. (B) Photographs of tape strips mounted onto silicon wafers. The visibility of sections at different thicknesses for wafer mounting and the alignment photo is shown on ccKapton (top) and CNT (bottom) at 50, 100 and 200 nm section thickness. (C) Mouse optic nerve sections at 30 or 50 nm thickness collected onto carbon coated Kapton (ccKapton) or CNT tape. Zeiss retractable BSD detector, 8 kV, 7.5 mm working distance. Scale bar 1 μm.

to evaluate the contact angle. Ideally, the water shows good spreading behavior with a contact angle below 45° (Fig. 5A). For more sophisticated tests a short tape strip (5 × 8 mm) can be used to fish single test sections, similar to sectioning on grid for TEM. The sections are in turn inspected by the target SEM acquisition parameters.

3.3.2 Materials

3.3.2.1 Equipment

- CNT tape or carbon conductive Kapton tape
- inverse forceps
- adhesive tape
- plasma discharger (easiGlow with custom-built vacuum chamber and motorization)
- empty reels

3.3.3 Step-by-step protocol

NOTE: Handle the tape and all materials with gloves to avoid any grease contamination.

NOTE: Be aware of the two sides of the tape: a conductive one (carbon- or carbon nanotube coating) and a non-conductive one. The sections are collected onto the conductive side. Plasma discharging is directional and should target this conductive side.

FIG. 5

Tape and ultramicrotome preparation. (A) Photographs of tape discharging unit. Self-made vacuum chamber with two tape reels and outside motor from the back (left). Note the twist in the tape (arrow). Plasma discharger from the front during discharge in the dark and with pump in the back (middle). Water drop on ccKapton before (top) and after (bottom) discharge (right) for hydrophobicity testing. (B) Photographs of tape insertion into the collector using forceps (first) and after correct insertion (second). Schematic drawing of the tape trajectory. The target tension setting is shown on the ATUMtome software (last image) (C) Ultramicrotome and collector photos (left, middle) with collector nose plunging into the knife boat and the ionizer positioned 3–5 cm from the knife edge (arrow). Screenshot of the ATUMtome software during sectioning with the ccKapton on the collector nose positioned 1.5 times the section length (arrow) away from the diamond edge (right). (D) Photos (left, middle) and technical drawing (right) of the custom-built ATUMtome enclosure (FMS-Montagetechnik, Bosch-Rexroth). The door is closed (left) or with opened (middle) window during the run and adjustments, respectively.

(1) OPTIONAL: Tape performance test
   (a) Cut a short (0.5–1 cm × 8 mm) tape strip and cut one corner off to introduce asymmetry in order to distinguish the conductive from the non-conductive side
   (b) Fix the tape strip using inverse forceps and fish a test ultrathin section from a diamond knife water bath
   (c) Mount the section on a silicon wafer with carbon adhesive tape (see Section 3.5), SEM-image at the strived acquisition parameters (see Section 3.6) and check for image quality and fold formation
(2) Take the end of the tape on a reel, twist it once and attach it to an empty reel using adhesive tape. This ensures that the inner (conductive) part is plasma discharged (Fig. 5A)
(3) Insert the tape reel on one shaft (left) and the empty one at the other (right) inside the vacuum box
(4) Close the box, check if the reels turn by shortly running the motor and start the vacuum pump
(5) As the self-made Plexiglass box is bigger than the manufacturer's, the target vacuum values are often not reached. Therefore, it is recommended to set a lower threshold value
(6) As soon as the vacuum is reached and the discharging is on (blue lightning) switch on the motor at a speed of 1 m/min
   NOTE: With slower speeds the conductive layer can be partially destroyed (and hence introduce charging artifacts) while running the tape too fast can lead to insufficient hydrophilicity (and cause collection wrinkles).
(7) Stop discharging at the end of the tape and vent the chamber
(8) Disassemble the tape and keep the orientation of the conductive, discharged side
(9) Rewind the tape to the initial reel by switching sides in the Plexiglass box and run the motor without vacuum and at high speed
(10) Check for hydrophilicity by dropping water on the tape and estimation of the contact angle (Fig. 5A)
(11) PAUSE POINT: Store the tape enclosed at RT in a petri dish for maximally 2 months

3.4 Serial ultramicrotomy

Timing: 2 h–1 d.

3.4.1 Principle

3.4.1.1 Decision for the right axial resolution

Before starting the serial sectioning procedure, it is important to decide on a target section thickness, which determines two crucial parameters: the axial resolution (Fig. 1) and the number of sections and thus the amount of wafers covering a given

tissue sample thickness. As ATUM-SEM was initially developed for "connectomics" research, a minimal axial resolution (29 nm; (Kasthuri et al., 2015)) was set to avoid overlooking of any synapse for lossless connectivity mapping. If ATUM-SEM is applied within a CLEM or other targeting experiments, the imaging procedure can be subdivided into a screening and the actual acquisition phase (Schifferer et al., 2021). In the first phase, thicker sections decrease the search time but reduce the axial resolution of the vEM data set. Usually, cell body (5–10 µm diameter) reconstructions can be achieved at 100–200 nm while thin glial processes require 30–80 nm axial resolution. Reconstructions of semithin (200–500 nm) serial sections result in three-dimensional representations with coarse morphological features.

We have combined ATUM-SEM screening of thicker, 0.5–5 µm sections with FIB-SEM acquisition of a region of interest to both, increase screening speed and at the same time render the entire sample block accessible to ATUM-SEM inspection (Kislinger et al., 2020b). FIB-SEM acquisition of the target structure enables high-resolution isotropic voxels (Kislinger et al., 2020b; Schifferer et al., 2021). The standard thickness for ATUM-SEM targeting projects that we present in this chapter is 80–100 nm as it nicely balances screening speed, contrast, conductivity as well as lateral/axial resolution.

3.4.1.2 Choice of diamond knife

The choice of the optimal diamond knife depends on the block face size and section thickness according to basic ultramicrotomy principle and the manufacturer's recommendations (Table 1). A special diamond knife with a bigger boat ("ultra maxi", Diatome, Powertome) can be purchased for ATUM-SEM applications. Water evaporates from the knife boat during longer ultramicrotomy sessions, which can be better compensated by a larger knife boat volume. However, we successfully worked with standard "ultra" knives with smaller boats for up to 2000 sections and regularly refilled water into the boat. In case of small sections (block face $<1 \times 1$ mm), a smaller boat can prevent sections from drifting away between tape nose and diamond edge and reduces water turbulences. The water pump can be adjusted to set constant water levels according to the manufacturer's suggestions. We usually observe the sectioning procedure entirely and prefer to manually adjust the water trough.

3.4.1.3 Environmental conditions

During ultramicrotomy, the general environmental conditions should be constant regarding temperature and humidity. In addition, any vibration and air flow should be avoided. The thinner the section the more sensitive is the ultramicrotomy toward these external parameters. In order to shield the ultramicrotome from environmental influences, RMC sells a plastic shielding. Based on this measure we designed a custom-built enclosure (FMS Montagetechnik) with a window and a door for stepwise opening. Setting up of the microtomy run is performed with open doors and adjustments during the run are made through the windows. For longer runs (>1000 sections) an antistatic device emitting both negative and positive ions (Static Line II, Diatome)

Table 1 Decisive aspects for serial sectioning.

Section thickness	**30–70 nm**	**70–200 nm**	**200–500 nm**	**>500 nm**
Knife	Ultra/ultra maxi 35°	Ultra/ultra maxi 35°	Histo	Heated ultra 35°
Tape	ccKapton	CNT or ccKapton	CNT or ccKapton	CNT or ccKapton
Block face edge length	**<1 mm**	**1–3 mm**		**>3 mm**
Knife	>3 mm edge	>3.5 mm edge		>4 mm edge
Collection	Short ribbons	Single sections		Single sections
Number of serial sections	**<500 sections**	**500–5000 sections**		**>5000 sections**
Knife	35° or 45°	35° or 45°		45°
Deionizer	Not needed	Beneficial		Needed

Depending on the section thickness (30–500 nm), different knife and tape types have to be chosen. The area of the tissue block affects the knife size and the number of collected sections impacts the knife angle and application of deionizer.

can be positioned at 3–5 cm distance from the cutting edge to avoid charging. This prevents worsening of the cutting performance of the knife and is especially useful for ultrathin sectioning (<50 nm). At closer distance to the knife edge the device creates some turbulences which possibly disturbs section collection. On the other hand, this ionizer flow can also support section separation from each other and the knife edge (Templier, 2019) (Fig. 5C).

3.4.2 Materials

3.4.2.1 Equipment

- diamond knife (ultra, ultra maxi, histo 35°, 45°, 3–4 mm)
- ultramicrotome with tape collector and software
- eyelash
- petri dish
- forceps
- adhesive tape

3.4.3 Step-by-step protocol

(1) Insert the tape while the collector is positioned at a distance from the microtome. Grab the tape by forceps and insert it into the lower and upper pinch rollers. The tension target should be set to ~2.8 by adjusting the jog forward and backward in the Powertome software (Fig. 5B). Once the tape reaches the empty reel, glue the end to the reel using adhesive tape

(2) Start with standard alignments and sectioning without tape collection until you reach the region of interest. Check if the microtome has been reset to exploit its entire feed range (200 µm)

OPTIONAL: If you want to collect from the very beginning move the collector in first

(3) Move the tape collector sideways to the level of the microtome. Adjust the position using the three set screws. While the collector nose is above the knife boat adjust its xy-position to be centrally behind the diamond edge, at approximately 1.5 times the distance of a section length (Fig. 5C). Then lower the nose to slightly immerse into the water without hitting the boat. Adjust the water levels to generate a more concave meniscus than for normal ultramicrotomy

(4) Move the sample block slightly away from the knife edge as the tape collector manipulation could have caused movements of the knife toward the sample. In the "ATUM" tab of the Powertome software (Fig. 5C) adjust the cutting window and section thickness. The cutting speed (0.5–0.8 mm/s) and the collection speed can be set equally. The tape speed during retraction can be reduced down to "0" in order to minimize spacing between adjacent sections on the tape

NOTE: Verify that the section is actually landing on the tape (Table 2).

Table 2 Trouble shooting serial ultramicrotomy.

Problem	Potential solutions
Sections rotate on the water bath and/or float away to the sides	Adjust the water levels Reduce the distance between collector nose and knife edge
Sections wrinkle during collection	Reduce the tape speed Glow discharge the tape
Sections vary in thickness	Close the enclosure and check for air flow, temperature variations or vibrations Adjust the water levels Clean the knife Install a deionizer (for longer runs)
Sections show chatter.	Turn the block by 90° Clean the knife
Sections are not collected onto the tape.	Change the angle of the tape collector nose Change the distance between collector nose and knife edge
Water levels fluctuate.	The automated water adjustment relies on edge detection at the water meniscus and therefore depends on the lightning conditions Adjust the water levels manually

(5) OPTIONAL: Install the deionizer at 3–5 cm from the diamond edge (Fig. 5C). This is recommended for longer sectioning runs, avoids charging of the knife and hence improves sectioning performance

(6) OPTIONAL: In the Powertome software choose the automatic water level adjustment using the peristaltic pump.

(7) Once the sectioning and collection has stabilized, close the windows and doors of the enclosure and observe the run through the camera (Fig. 5D). Adjust parameters in the software if needed.

NOTE: In case other adjustments are necessary, do all handling through the enclosure windows. Observe sectioning at all time and avoid breaks.

(8) OPTIONAL: Markings can also be made on the run to label features that can already be extracted during microtomy (e.g., full tissue section reached). Use a foil pen and label the edge of the tape during retraction or by stopping the microtome. This narrows down the site of interest in the lateral dimension and saves time and material in the subsequent mounting step

(9) In order to stop the run set the section thickness to "0" while continuing collection. This kicks the last section of the diamond edge onto the tape while no new section is generated. Open the enclosure, label the tape after the last collected section using a marker. Increase the collection speed and watch the marking until it reaches the tape reel. Cut the tape and store the reel in a petri dish

NOTE: Marking is not possible if the tape is extremely hydrophilic.

3.4.4 Optimization and trouble shooting

Potential problems and suggested solutions concerning serial ultramicrotomy on tape are listed in Table 2.

3.5 Wafer assembly

Timing: 1 h–1d.

3.5.1 Principle

After ultramicrotomy the tape bearing sections has to be mounted on a silicon support. Silicon wafers are commercially available, fit into special SEM holders and can be mapped using SEM imaging software. Wafer mounting can be performed on a normal bench or using the wafer workstation (RMC) with additional top lights and templates for tape strip lengths. Nine tape strips with sections can be mounted onto three carbon adhesive tape strips.

3.5.1.1 Section visibility

Top lighting is especially important for sections thinner than 70 nm on CNT tape as their visibility is limited (Fig. 4B). The ability to clearly see the sections is a prerequisite to avoid cutting through a section. In this regard, CNT tape performs worse than ccKapton (Fig. 4B).

3.5.1.2 Serial section order

There are two ways to keep the right section order and orientation: either the last section is glued to the end (right bottom) of the wafer. Alternatively, the tape roll is rewound onto an empty reel and the tape is glued to adhesive tape starting with the first section (top left on the wafer). The sections are adhered onto three 2.5 cm wide carbon adhesive tape strips, resulting in 9 tape strips with sections. Usually 200–300 sections fit onto one wafer. The tape has to be grounded by carbon adhesive stripes or silver paint all along the tape length in order to avoid charging (Fig. 6A and B). Throughout mounting, it is important to take care of the orientation of the tape, regarding the section-facing side versus the empty back side.

3.5.1.3 Cleanness and storage

Throughout the entire mounting process (Fig. 6A and B) it is key to keep the wafer dust- and grease-free. We use a compressed air duster and 80% ethanol to clean the preparation area and wear gloves at any time. Wafers are stored in rectangular, 10 cm petri dishes and fixed with two stripes of copper tape at two ends to the inside of the lid. CD boxes are space saving alternatives (Baena et al., 2019). For long-term storage, desiccator cabinets or—as a cheaper option—closed plastic boxes with desiccant pads (rice, silica gel) are recommended. The tapes and sections are a potential source of contamination in the SEM chamber. Initially, we observed image shifts between the hierarchical imaging rounds. In order to reduce these artifacts which limit imaging and reimaging capabilities, wafers are outgassed and precleaned before loading into the SEM using a custom-built, heatable vacuum chamber (WF100, Binder Labortechnik, Science Services) (Fig. 6C and D). We recommend cleaning the empty SEM chamber by plasma discharging after 10–20 wafer exchanges.

3.5.2 Materials

3.5.2.1 Equipment

- OPTIONAL: wafer preparation station (RMC)
- Compressed air duster
- Tape reel
- Tape dispenser
- OPTIONAL: 50 mL falcon tube, filled water bottle 1 L
- roller
- petri dishes
- 2 forceps
- scissor/scalpel, razor blade
- copper adhesive tape
- OPTIONAL: wafer drying station (Binder, Science Services)
- silicon wafer, 4″, 1-side polished, p-type (Boron), 1–0 Ohm cm
- carbon adhesive tape
- copper adhesive tape
- soft carbon adhesive tape
- silver paint or soft carbon adhesive tape

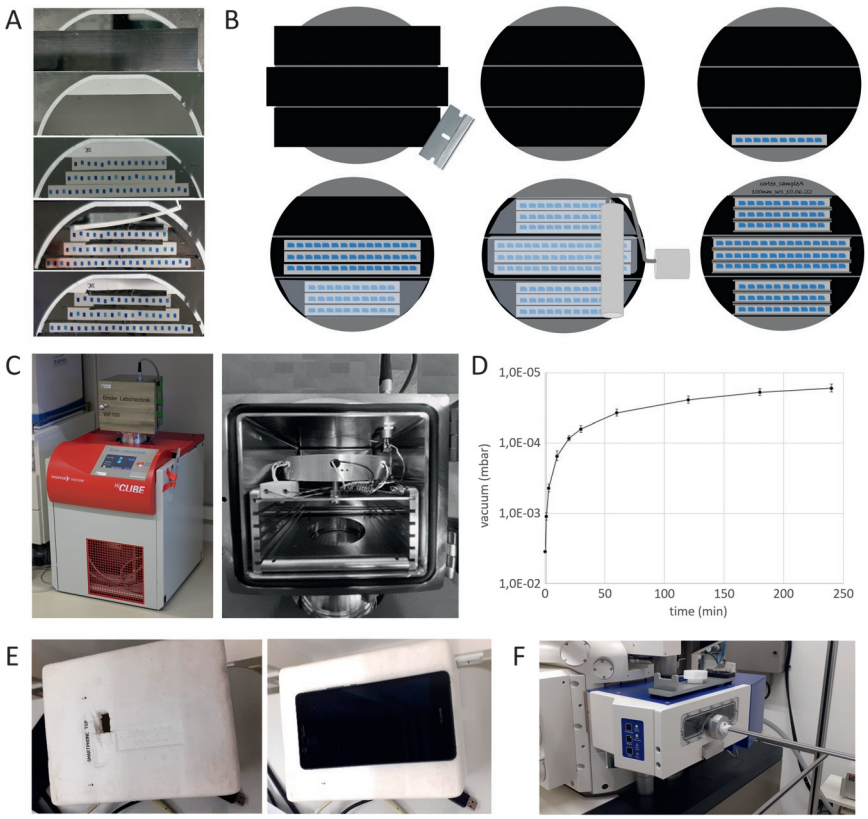

FIG. 6

Wafer preparation. (A) Photographs of different wafer preparation steps (top to bottom): wafer with carbon adhesive tape, edges cut off, ccKapton with sections, carbon adhesive strips with covering paper, covering paper removed. (B) Schematic drawing of wafer preparation. Silicon wafer (gray), carbon adhesive tape (black), blue (section), tape (orange), plastic cover of carbon adhesive tape (light blue), carbon conductive tape (white). (C) Wafer drying (WF 100, Binder, Science Services) station from outside (left) and inside with multiple shelves for wafers (right). (D) Outgassing of prepared wafers at room temperature ($n = 3$) in the wafer drying station. (E) Custom-made wafer photo stations for mobile phones without (left) and with a mobile phone with camera (right). (F) Airlock system for the transfer of 4 in. wafers into the SEM (Crossbeam 340, Zeiss).

- plastic storage box with lid
- desiccant or rice
- OPTIONAL: sputter coater with glow discharge unit

3.5.2.2 Reagents

- ethanol
- OPTIONAL: uranyl acetate
- OPTIONAL: stabilized lead citrate

3.5.3 Step-by-step protocol

NOTE: Wear gloves in order to avoid grease contamination.

(1) Clean the wafer using a compressed air duster and ethanol

(2) OPTIONAL: rewind the tape. An empty reel is deposited onto a falcon tube attached to a tilled water bottle. Attach the end of the tape to the empty reel using adhesive tape. Manually rewind the tape

(3) Cut three strips of carbon adhesive tape that cover the wafer. Remove the white paper from one side of all strips and attach them onto the shiny side of the wafer. Avoid overlap of the strips

(4) Remove the overhanging carbon adhesive tape edges using a razor blade (Fig. 6B)

(5) Attach the 4-in. silicon wafer to the wafer working station (RMC) using copper adhesive tape

(6) Remove the plastic cover of the bottom carbon adhesive tape and keep it

NOTE: If the tape is not rewound (see Section 2) start with attaching the last section to the right bottom of the wafer. This way the first sections will be placed at the upper left part of the wafer.

(7) Position the tape reel onto the tape dispenser and put it next to the wafer preparation station. Make sure that the lighting enables section visibility (especially for CNT tape, Fig. 4B)

(8) Grab the CNT/Kapton tape with using forceps and cut it between two sections to a length that fits onto the bottom row of adhesive carbon tape

(9) Using two forceps transfer the cut strip and attach it to the adhesive tape

NOTE: As the attachment is irreversible carefully estimate the distance to both ends and start the attachment in the middle. All sections outside the adhesive tape are lost. Avoid regions of detachment as major charging problems could arise.

(10) Continue to fill the bottom adhesive tape region with three tape strips. Put the plastic cover back on top of the three section strips (Fig. 6A and B). Continue with the rest of the wafer until all nine stripes are placed

(11) Use miniature wallpaper roller, rolling pin or similar to flatten the strips with gentle pressure (Fig. 6B). The air bubbles should be removed while avoiding squeezing the sections by applying brute force. Check the result and manually correct any detachment. The plastic covers can be removed as soon as all stripes are properly attached. Any detachment can lead to charging or variations in working distances between sections (Fig. 7K)

(12) Cut 1–4 mm strips, several mm longer than the attached tape, from soft carbon adhesive.

(13) Grab the soft carbon adhesive strips by two forceps at both ends and position it between CNT/ccKapton and carbon adhesive tapes. Repeat this for all nine strips. The soft carbon tape covers two CNT/ccKapton tape strips except at the two marginal strips. Finally, remove the white protective paper (Fig. 6A)

NOTE: Never position tape onto a section.

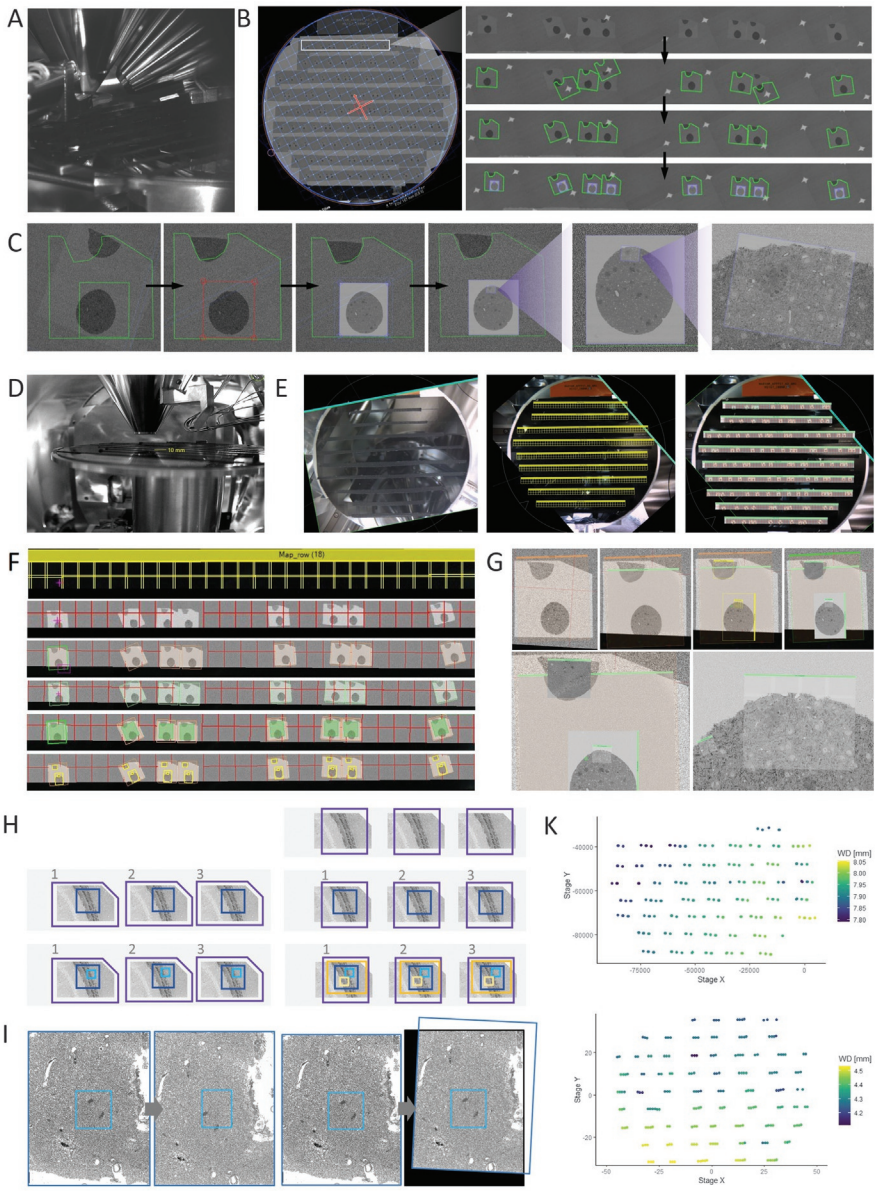

FIG. 7

Wafer mapping by Atlas 5 (A–C) and Maps 3 (D–G). (A) Chamber photo. (B) Wafer overview scan generated in Atlas 5 at $1.5 \times 1.5\,\mu m$ pixel size. The red cross indicates the stage position and the box highlights the sections shown at the right side. Eight 100 nm thick sections on a single tape strip shown at different steps in the mapping process (from top to bottom) starting with the low-resolution overview scan image, the automated stamping of section outlines, its correction and with the regions chosen for medium resolution

(14) OPTIONAL: The soft carbon adhesive tape (steps 12–13) can be replaced by silver paint

NOTE: Silver paint evaporation can contaminate the microscopy chamber.

(15) For documentation, add a written label using an overhead marker at the blank silicon part at the top

(16) OPTIONAL: Glue TEM grids onto the carbon adhesive tape. These can be used for wafer mapping in case a photo (acquired in a custom-made Styrofoam or similar box) is used for navigation (Fig. 6E)

NOTE: This is especially advantageous in the Maps acquisition workflow.

(17) Place the wafer into a big petri dish and attach it with copper adhesive tapes at the two blank silicon sides onto the petri dish lid

---

(200 × 200 nm) acquisition in (violet). (C) Mapping and acquisition steps shown for one section as an example. From left to right: wrong section site mapping (green outline) with wrong positioning of the ROI for medium resolution acquisition (green inset); corrected mapping with right positioning of the medium resolution ROI (red); acquired medium resolution ROI (violet), acquired high resolution ROI within the medium resolution ROI and high magnification images thereof. (D–G) Wafer mapping by Maps 3. (D) Chamber image. (E) Whole wafer screenshots: Nav-Cam picture (left), aligned with SEM beam with imported rows (middle), and acquired overviews (right). (F) Screenshots of a tape row with eight sections in consecutive steps of the AT workflow in Maps 3. From top to bottom: row-mapping tile set (yellow grid) on Nav-Cam image before acquisition (1); acquired row-mapping tile set after T1 detector acquisition (1.5 × 1.5 μm pixel size) (2); unordered section outlines (orange) (3); ordered section outlines (green) (4); T1-detected section previews with successful position refinement (success is indicated by green refinement region, 400 × 400 nm pixel size) (5); focus and ROI array tile sets for acquisition (6). (G) Maps 3 mapping and acquisition steps shown on one section. Upper row from left to right: Section outline detected through pattern matching (orange outline) (1); section outline and T1-acquired section preview (green outline) (2); focus and ROI array tile sets to be acquired per section (yellow outlines) (3); array tile sets after successful acquisition (green outlines) with close up views in the lower row with the coarse focus region (tissue on top of section) and fine focus region (in the lower tissue part, left of the target region). (H) Comparison of the Atlas 5 (left) and Maps 3 (right) workflows. Schematics of the steps in the mapping workflow. Violet boxes indicate the area selected for the section assignment, blue the medium and cyan the high-resolution site. In contrast to Atlas 5 (left), there is a fully automated section detection function in Maps 3 (right). The order of the sections has to be assigned manually. (B) Maps 3 lacks the "checking" option to set starting values for focus and stigmation and highly benefits from coarse (dark yellow) and fine (light yellow) autofunction tile sets. (I) Software screenshots of scanned cortical tissue. The cyan box indicates the automated positioning of the section site. Atlas 5 (two left images) simply signs the relative coordinates within the section set while the Maps 3 (two right images) positioning is feature-dependent. (K) Spatial distribution of focus heights as analyzed from the working distance (WD) values extracted from the autofocus results on the actual image (top, Atlas 5) or the fine focus region (bottom, Maps 3).

(18) OPTIONAL: Wafer poststaining. For blocks with little heavy metal load (e.g., non-rOTO stained TEM samples) the sections can be poststained on the wafer (Morgan et al., 2016)
- **(a)** Glow discharge wafer for 15 s in a glow discharger (Quorum sputter coater Q150T) for the reagents to spread nicely on the tape thereby reducing the reagent volume needed
- **(b)** Place the wafer in a big (14 cm) diameter petri dish and dispense 4% uranyl acetate through a syringe filter onto the CNT/Kapton tape strips until all sections are covered. Incubate for 4 min. Protect the sample and the reagent from light
- **(c)** Immediately immerse the wafer in another big petri dish filled with ~100 mL distilled water. Using forceps lift the wafer up and down on one side while the opposite side stays at the bottom of the petri dish. Then, rotate the wafer by ~120° and repeat the up-and-down movement. Repeat the 120° rotation
- **(d)** Dry the wafer thoroughly using a deduster
- **(e)** Apply 3% stabilized lead citrate (Ultrostain, Leica) onto the tape using a filtered syringe. Incubate for 4 min
- **(f)** Wash in water and dry (see c and d)

(19) The assembled wafer is documented by indicating sample name, section thickness, wafer number and date

(20) OPTIONAL: Decontaminate the wafer in the wafer cleaning station (WF 100) at RT overnight

PAUSE POINT: Keep the wafer in a closed plastic box until the imaging session. Place a bag with desiccant or rice into the box to keep it dry.

3.6 Serial section image acquisition

Timing: 1d–3w.

3.6.1 Principle

3.6.1.1 Mapping software

The serial section image acquisition procedure highly depends on the chosen SEM software. To our knowledge, there are four different providers of AT software for SEM serial section imaging: Zeiss (Atlas), Thermo Fisher Scientific (Maps), Hitachi (ACAT, Automated Image Acquisition System for Serial Section Analysis) and Jeol (SEM Supporter). Here, we demonstrate and discuss the workflow, using two alternative software packages, Atlas 5 (Zeiss, Fibics) and Maps 3 (Thermo Fisher Scientific) for the respective microscopes available in our laboratory, Crossbeam 340 (Zeiss) and Apreo S2 (Thermo Fisher Scientific) (Fig. 7, Table 3). In theory, any other single beam instrument with BSD or SE detection systems would be suitable. A dedicated mapping- and serial sectioning software is very useful but not

Table 3 Comparison of Maps 3 and Atlas 5 software packages.

	Atlas 5	Maps 3
Mapping		
Mapping template	Photo, wafer overview scan	Photo, NavCam, wafer overview scan (in combination with NavCam)
Detector wafer overview scan	BSD, SE2	T1, SE2
ROI for wafer overview scan	Whole wafer	Tape strips
ROI detection within section	Manual (fixed coordinate)	Automated (feature-dependent)
Serial section imaging		
Detector and settings	Retractable BSD, 8 kV, 7–8 mm WD, 60 µm aperture	T1, 1 kV, 4–5 mm WD, 0.2–6.4 nA beam current (high-low resolution settings), beam deceleration
Autofocus/−stigmation region	Center	Adjustable
Autofunction starting value	Manual adjustment ("check protocols")	Non-adjustable; automated by additional focus tile sets
Selection of every other section for imaging	Manual, reversible selection within a given site	Manual, irreversible deletion of individual sections in a tile set array
Selection of certain range of images (24–73 instead of 1–100)	Simple selection	Simple range restriction (slider)
Parameters overview imaging	100–200 nm/pixel, 0.6–1 µs dwell time	200–450 nm/pixel, 0.2–3 µs dwell time
Parameters medium resolution imaging	20–50 nm/pixel, 1–2 µs dwell time	10–50 nm/pixel, 2–3 µs dwell time
Parameters high resolution imaging	4 nm/pixel, 2–3 µs dwell time	1–3 nm/pixel, 3–5 µs dwell time
Image postprocessing		
Stitching	Manual, automated	Manual, automated
Alignment	Automated	–

essential. Beyond the commercial solutions, the WaferMapper software was developed for Thermo single beam SEMs (Hayworth et al., 2014). The imaging run starts with the mapping of a wafer photo acquired in a suitable box (custom-built Styrofoam or photo box, Fig. 6E) or an overview SE/BSD detection scan in order to be able to navigate on the wafer and define regions with tape strips and, ideally and more precisely, section outlines. The software is used to identify sections and assign their sequence. Imaging at increasing resolution schemes is performed either in several rounds on all selected sections (Atlas 5) or in one session, hierarchically within one section (Maps 3) (Fig. 7, Table 3). This is enabled by the assignment of protocols to selected regions which apply a defined pixel size, dwell time, auto functions (focus, stigmation, brightness and contrast), tile size and other parameters. After acquisition, there are

postprocessing options including stitching and alignment that can be done at the microscope PC using the acquisition software. The acquisition typically takes several days to weeks and is monitored remotely.

Even though both imaging software packages are applicable to the majority of samples, there are differences regarding the degree of automation (Fig. 7, Tables 3 and 4). Maps 3 integrates more automated steps than Atlas 5, e.g., the section recognition step. However, manual correction takes computing power and is more time consuming in Maps 3 (Table 4). Automated image processing including ROI recognition and autofocus functions is especially challenging if the structure of interest is surrounded by empty resin (e.g., blood vessels, brain ventricles, cell culture) or if characteristic features are missing (Table 4).

3.6.1.2 Detectors

The choice of detector and respective settings are quite variable but has to be adapted to the particular needs and available instrumentation. In general, SE detectors enable fast acquisition while BSD detectors are less prone to charging and surface artifacts and can be used for carbon-coated sections (Fig. 4A). Detector that enable large field of view inspection are preferred for overview mapping. Limited tile sizes can introduce stitching artifacts and slow down the acquisition.

3.6.2 Materials

3.6.2.1 Equipment

- Wafer box
- Wafer holder (Zeiss)
- Wafer holder (Thermo Fisher Scientific)
- Single beam SEM (Crossbeam 340, Zeiss; Apreo S2, Thermo Fisher Scientific)
- Array Tomography Software (Atlas 5, Fibics/Zeiss; Maps 3, Thermo Fisher Scientific)

3.6.3 Step-by-step protocol

3.6.3.1 Option A: Atlas 5

OPTIONAL: Take a photo of the wafer for mapping purposes. Use a Styrofoam box with a hole at the bottom (Fig. 6E) (alternatively, a photo box, Ralph Neujahr, Zeiss, personal communication). Invert the box onto the wafer and position a mobile in such a way that the wafer can be imaged through the whole of the box. Acquire an image and use the photo for an additional alignment step in Atlas.

(1) Position the wafer onto the wafer holder and introduce it via the airlock system (Fig. 6F)

SmartSEM software

(2) Introduce the retractable BSD detector, position the wafer and adjust the working distance to 7–8 mm (Fig. 7A). Set the beam to 6–8 kV and use a 30–60 µm aperture

Table 4 Troubleshooting acquisition software.

Problem (Maps3)	Potential solutions
Charging artifacts emerge during imaging	Use the compound lens filter, which, however, introduces notable spherical aberration especially for large tiles
	Make sure that the autofunction tile sets are placed outside the ROI
	Adjust the rOTO protocol or perform staining on sections already mounted on the wafer (adding more heavy metals) (see Section 3.1)
False positive, misplaced or negative sections during automated section detection. (Manual adjustment is slow and thus time-consuming.) (step 7)	Select another, more prototypical section as a template. If the first section is damaged consider placing it at position two or three, since position one will be used as a template for position refinements
	Include characteristic features such as upper and lower section borders or a trimmed edge. This can support the correct automated section detected in terms of rotation
	Try to avoid inclusion of the left and right section borders if you have cut ribbons since these edges may not be universal to all sections (Fig. 7H)
	Change the maximum number of detected sections to a high value (300 to 30.000.000) and adjust the detection threshold in case of unacceptable amounts of false positives/negatives
	Reacquire the overview mapping strips (step 6) with increased dwell time (>1 μs). Higher signal to noise ratios are more beneficial than smaller pixel sizes
The preset tile set parameters of the first section preview do not meet your needs. (step 8)	Start the first section preview acquisition. Stop the imaging after at least one tile has been acquired and reset its acquisition. This enables you to choose freely all tile set parameters. Choose run ("play" button) instead of "cquire section preview" in order to apply the changes. Once the first preview is imaged, "acquire all section previews" will take over the chosen parameters
Imaging the whole section for the preview is too time consuming. (Movements of the preview outline on the first section will not apply to other sections. Tiled section previews can cause problems at later position refinement steps.) (step 8)	Reduce the size of the section template in step 7. Note that a smaller template size reduces characteristic features needed for the autodetection
	Choose one of the big squared tile resolutions (>10 k × 10 k pixels) in combination with the reduced window function
Position refinement fails for many sections or starts to drift. The "continue position refinement" function can crash the software or introduce errors	Manually adjust the misalignments (time-consuming)
	Choose a different refinement area that is found on every section
	Improve the section preview image quality by increasing the dwell time and resolution
	Skip the refinement step and adjust manually if sections vary very much (e.g., folds)
High-resolution tile sets appear non-focused or stigmated	Make sure the autofunction tile sets cover tissue and not empty resin
	One of the autofunctions was out of range. Defocus manually and run a test of all focus tile set settings (to microscope) in order to identify which level failed. Increase the working distance step in the setting (as a starting point: if pixel size >20 nm: WD-Step = pixel size x 100; if <20 nm: WD = 1 μm)
	The signal-to-noise ratio was not high enough. Adjust pixel dwell time or line average of the failing autofunction tile set
	The image shifts during focusing. Check the beam alignments, especially the focus alignment or increase the width of the reduced focus area and/or use a square
	Autostigmation failed. If stigmation fails once, usually all of the following tile sets will be stigmated. As fixed stigmation values cannot be set, consider omitting autostigmation whenever possible

Atlas 5 software

(3) Start a new project and acquire an overview scan of the wafer by BSD detection (Fig. 7B). Generate a round shape covering the wafer and select a protocol with 2–5 µm/pixel, 0.8 µs dwell time. Check the region and start imaging (~1.5 h)

OPTIONAL: Use the photo and image three characteristic sites on the wafer (e.g., TEM grids) to perform an alignment.

(4) Generate a shape that exactly surrounds the first section. Move the shape to the first section (top left) and choose one of the two stamping tools to generate a section set (Fig. 7B). Using the manual stamping tool select the position and rotation of the following sections as precise as possible

OPTIONAL: For the semi-automated stamping tool choose a typical section (from the center of the wafer) without neighboring ones. Correct the wrongly assigned sections manually.

(5) Image the section set or choose a subregion by generating a site within the section (Fig. 7C and H). Choose a protocol that meets your image quality needs in order to relocate certain structures. Typically, a pixel size of 50–200 nm at 1–2 µs dwell time is sufficient. Check all sites or the sites at the beginning of a new tape strip. This determines the contrast and brightness (important if section thickness varies) as well as the starting focus for the autofunction (several hours—1 to 2 days)

NOTE: Autofocusing is needed, autostigmation is usually not necessary and potentially causes beam damage (Fig. 10E).

NOTE: As the focal point varies mostly between very distant sections and the sections are ordered in a serpentine way, the transition between tape strips is most critical. In case of air bubbles or unevenness of the tape, the focal point also varies between adjacent sections on the same tape (see Section 3.5.3, Fig. 7K).

NOTE: While the section set covers every section it is possible to choose individual sites for medium resolution acquisition. For screening purposes it might be sufficient to image only every other, 5th, 10th, etc. section.

(6) The generated medium resolution images enable the identification of the ROI (Fig. 7C and H). Select the section numbers as well as the exact lateral position for the high-resolution acquisition. The sites have to be positioned manually to fit the ROI on each section as the software only assigns the relative coordinate of the site within the section set without any feature recognition. Choose the pixel size (3–20 nm) and dwell time (2–3 µs) for the high-resolution acquisition and "check" focus, brightness and contrast for every section or at least every new tape strip.

NOTE: For the identification of ROIs it might be required to first reconstruct the medium resolution data set (Herwerth et al., 2022).

NOTE: Correct the alignments if the image shift between different resolution settings is bigger than the stage movement error (~4 µm). Usually, the image shift is reduced if the medium resolution is more similar to the high-resolution settings and if the time offset between these two imaging rounds is reduced.

(7) Inspect the section set for properly focused images (Fig. 7K) and reacquire.

3.6.3.2 Option B: Maps 3

(1) Position the wafer onto the wafer holder and introduce it via venting the system (Fig. 7D)

xT software

(2) Acquire a Nav-Cam image (Fig. 7E) during system evacuation

(3) Position the wafer and adjust the working distance to 4.5–5 mm. Use the T1 Inlens detector. Set the beam to 1–2 kV and use a 0.1 to 0.2 nA aperture. Use the Optiplan lens and set the beam deceleration to 2–3 kV

Maps 3 software

(4) Start a new project and import the Nav-Cam image

(5) Align the Nav-Cam image. Choose three widely spread characteristic points identifiable on the Nav-Cam and the EM image (e.g. label letters, edges of conductive carbon adhesive strips, TEM grids). Acquire snapshots at the selected positions using the T1 detector and align these SEM images with the Nav-Cam photo using the three-point alignment workflow in the software

(6) For generating overview images of the strips, create one individual tile set for each strip and place it in such a way that it covers all sections with some surplus (Fig. 7E). Use settings that provide sufficient signal to noise ratio for consecutive section detection while maximizing the field of view. (1.8 µm/pixel, 500 ns pixel dwell time, 1024×884 pixels).

(7) Start the "array tomography" workflow with section detection (while skipping the wafer mapping step (step 1)). Draw a box around a prototypical section (Table 4, Fig. 7F and G). Remove false positive section outlines, add missing ones and correct pronounced rotation errors

(8) Assign an order to the sections using the line tool (Fig. 7F and H). Correct any mislabeling by redrawing the line through the section and including some prior and posterior sections

(9) Create section previews

OPTIONAL: If you want to change the tile parameters, acquire the first section preview and immediately reset the acquisition afterwards. Choose the settings in a way that allows for imaging of the whole section without tiling and result in high signal to noise ratio (typically 200 nm pixel size, >12 k image size, 2 µs pixel dwell time). Use the reduced window function if only a subset of the whole section is of interest. Set a coarse autofocus (Table 5). Press the run button on the bottom to acquire the first section preview (pressing "acquire first section preview" will reset all prior adjustments).

(10) Center the view on the first section and choose a region with characteristic features for the position refinement step. Correct remaining alignment errors manually

NOTE: Smaller regions closer to the exact ROI may achieve higher quality alignments but are more error prone.

(11) Create tile set arrays and choose the acquisition order option "per section" and "acquire all arrays"

Table 5 Autofunction parameter in Maps 3.

Tile set array	Auto function step	Dwell time	Reduced area location	Relative HFW	Resolution	WD Step
Coarse focus	Focus	>8 µs	Big centered stripe (width:5% of image size)	Multiple of tile pixel size to get ~1.5 µm pixel size during focus	1024 × 884	150.000 µm –180.000 µm
	Focus after lens alignment	5 µs	_"_	multiple of pixel size to get ~200 nm pixel size during focus	_"_	20.000 µm – 50.000 µm
Fine focus and stigmation	Focus	3 µs –5 µs	Centered box or stripe similar to above	1 (if desired pixel size >10 nm) or 2	_"_	1.000 µm – 2.000 µm
	Stigmator	5 µs	Centered preset box	–	_"_	–
	Final focus	3 µs	Centered box or stripe similar to above	1	_"_	1.000 µm

OPTIONAL: Include three autofunction tile sets (Fig. 7G and H) in order to account for working distance variations across the wafer (Fig. 7K). Set the resolution to 1024 and choose decreasing pixel sizes (coarse, medium, fine), ending with the resolution for the actual ROI (Table 5). Test all autofunctions before acquiring the tile set arrays and place the fine autofunction tile set array as close to the ROI as possible. Make sure that the autofunction tile set arrays are positioned within tissue regions but not in the ROI.

3.6.4 Optimization and troubleshooting

Problem (Atlas 5)	Potential solutions
Semiautomated section detection is incorrect (not positioned around sections but at random sites) (Fig. 7I)	Select a prototypical section as a template
	Choose the manual section detection option, especially if single sections and ribbons alter
	Cut single sections instead of ribbons.
	Trim at a steeper angle (see Section 3.2)
	Check for section thickness variation and minimize environmental disturbance during sectioning (see Section 3.4)
High-resolution images are not focused	"Check" each site before the acquisition as the focus can highly alter, even between neighboring sections
	Make sure that the tape strips are properly grounded by carbon adhesive tape or silver paint
	Reposition the region of interest if the center doesn't contain any features suitable for auto-adjustments
	Autofocus region bleaches. Add more heavy metals during sample preparation or poststain the wafer
	Adjust the autofocus/−stig parameters and use the test option
Image shifts between the low-, medium- and high-resolution sites	Realign the beam
	Choose a medium focus site with a pixel size closer to the high-resolution one
	Choose the ROI big enough to account for stage inaccuracy (~4 μm)
Central autofocusing region is visible in the high-resolution image	Shift the region of interest out of the center to avoid tissue destruction at the autofocus site
	Add more heavy metals during sample preparation or poststain the wafer

3.7 Image registration

Timing: 1 w–6 m.

3.7.1 Principle

Section registration is facilitated in FIB-SEM or SBF-SEM as the orientation of the remaining block face is stable. In contrast, ATUM and other AT techniques are prone to translation, rotation and distortion (folds, stretching) of collected sections which has to

be corrected during alignment. Furthermore, ATUM shows higher inter-section thickness differences as the ultramicrotomy step is not shielded within a SEM chamber like in block face techniques but is influenced by environmental conditions. In turn, this variability leads to inter-slice histogram variation. Overall, section collection techniques result in image series with higher heterogeneity, thus complicating registration.

For details of image registration, segmentation and rendering we refer to the rich information about the respective software, especially Fiji/TrakEM2 (Cardona et al., 2012; Schindelin et al., 2012), VAST (Berger et al., 2018) and Blender, respectively. Here, we solely describe a manual way of registration using built-in Maps 3 or Atlas 5 features.

3.7.2 Materials

3.7.2.1 Equipment

- OPTIONAL: Atlas 5
- OPTIONAL: Maps 3

3.7.3 Step-by-step protocol

A. Stitching and registration in Atlas 5

1. Select the batch stitching option. The results can be checked and manually adjusted if needed.
2. Select the alignment of the section site and export the stack as single tiff files. NOTE: These procedures may be slow if Atlas 5 is run on the microscope PC.

B. Stitching in Maps 3

If the unstitched data was created via the AT-workflow and is an Array tile set, batch stitching is available as a right click option 'Stitch all' of the array tile set in the project tree. It can be started automatically or manually.

NOTE: Registration is currently not available in Maps 3 and can be done in Fiji.

4 Key resources table

REAGENT or RESOURCE	Source	Identifier
Chemicals, Peptides, and Recombinant Proteins		
Glutaraldehyde	Science Services	Cat# E16216
Silver paint Leitsilber, Acheson 1415	Plano	Cat# G3692
LX112 Embedding Kit	LADD Research Laboratories	Cat# 21210
Osmium tetroxide	Science Services	Cat# E19130
Paraformaldehyde	Science Services	Cat# E15713
Potassium hexacyanoferrate(II) trihydrate	Sigma-Aldrich	Cat# 455989
Sodium cacodylate trihydrate	Science Services	Cat# E12300
Thiocarbohydrazide	Sigma-Aldrich	Cat# 223220

—cont'd

REAGENT or RESOURCE	Source	Identifier
Uranyl acetate	Science Services	Cat# E22400
Ultrostain II (3% stabilized lead citrate)	Leica Microsystems	N/A
Experimental Models: Organisms/Strains		
wt mice	The Jackson Laboratory	C57BL/6J
APP/PS1 mice	Mathias Jucker (Radde et al., 2006)	http://www.informatics.jax.org/allele/MGI:3765351
Twitch2b-YFP mice	Oliver Griesbeck (Thestrup et al., 2014; Witte et al., 2019)	N/A
Software and Algorithms		
SmartSEM	Carl Zeiss Microscopy GmbH	N/A
Atlas 5, Array Tomography, 3D	Fibics Incorporated, Canada	N/A
xT	Thermo Fisher Scientific	N/A
Maps 3.19	Thermo Fisher Scientific	N/A

5 Materials and Equipment

Plastic handle knives	Science Services	Cat# 72006–02/03
Ultramicrotome equipped with an ATUMtome including Powertome, ultra maxi 4 mm 35° diamond knife (Diatome), anti-static device (Diatome), air-activated anti-vibration table with compressor, environmental chamber, water level control system, wafer workstation	RMC Boeckeler, Science Services	Cat# R-ATUMtome
Binocular	Kern & Sohn GmbH	Cat# OZL 464
Silicon wafer, 4″, 1-side polished, p-type (Boron), 1–0 Ohm cm	MicroChemicals	Cat#
WSM40525200P1334SNN1		
Carbon-coated double sided adhesive tape	Science Services	Cat# P77819-25
Carbon nanotube tape (CNT TPEN, Typ TEI, 8 mm wide)	Science Services	Cat# R-ATUM313

Continued

—cont'd

Plastic handle knives	Science Services	Cat# 72006–02/03
Kapton tape	Science Services	Cat# ATUMtape308GD-30
Carbon coated Kapton tape	Jeff Lichtman, Richard Schalek (Schalek et al., 2012)	N/A
Syringe filter 0.2 µm	VWR	Cat# 514-8058
Wafer drying station	Binder Labortechnik, Science Services	Cat# WF 100
PELCO BioWave Pro+ with ColdSpot, EM Pro vacuum chamber, SteadyTemp pro	TED PELLA	Cat## 36700-230 36116-10, 3535, 50062
Standard oven (e.g., Incu-line IL 10)	VWR	Cat# 390-0384P
Universal sample holder	Leica	Cat# 16701761
Diamond knife ultra 35°, 45°, 3 mm	Diatome/Science Services	Cat# DU3530; DU4530
Diamond trimming knife trim 90	Diatome/Science Services	Cat# DTB90
Glass vial with rolled rim, short (5 mL), with lid	Carl Roth	Cat# CLA1.1
Empty tape reel	Science Services	Cat# R-ATUMspool
Universal sample holder	Leica	Cat# 16701761
CNT PET tape	Science Services	Cat# R-ATUM 312–40
Crossbeam 340 (or another single beam SEM)	Zeiss	N/A
Apreo S2	Thermo Fisher Scientific	N/A
Holder for 4 in. wafer	Zeiss	Cat# 348242-8247-000
Wafer holder	Thermo Fisher Scientific	Cat# FP3660/14
UC7 ultramicrotome	Leica Microsystems	N/A

6 Expected outcomes

We exemplify the ATUM-SEM workflow and its strengths for targeting specific pathologies (1) and performing correlated ultrastructural reconstructions (2).

First, we show the application of ATUM-SEM for the three-dimensional rendering of amyloid plaques in in the APP/PS1 mouse model of Alzheimer 's disease (Fig. 8). Plaques consist of a core with extracellular β-amyloid surrounded by degenerating neuritic processes (Fig. 8C). The core and dystrophic neurites are contacted by phagocytosing microglia containing lysosomes (Fig. 8D). Typically, in mice at 6 months of age, plaques of 50–100 µm diameter can be found in the APP/PS1 cortex

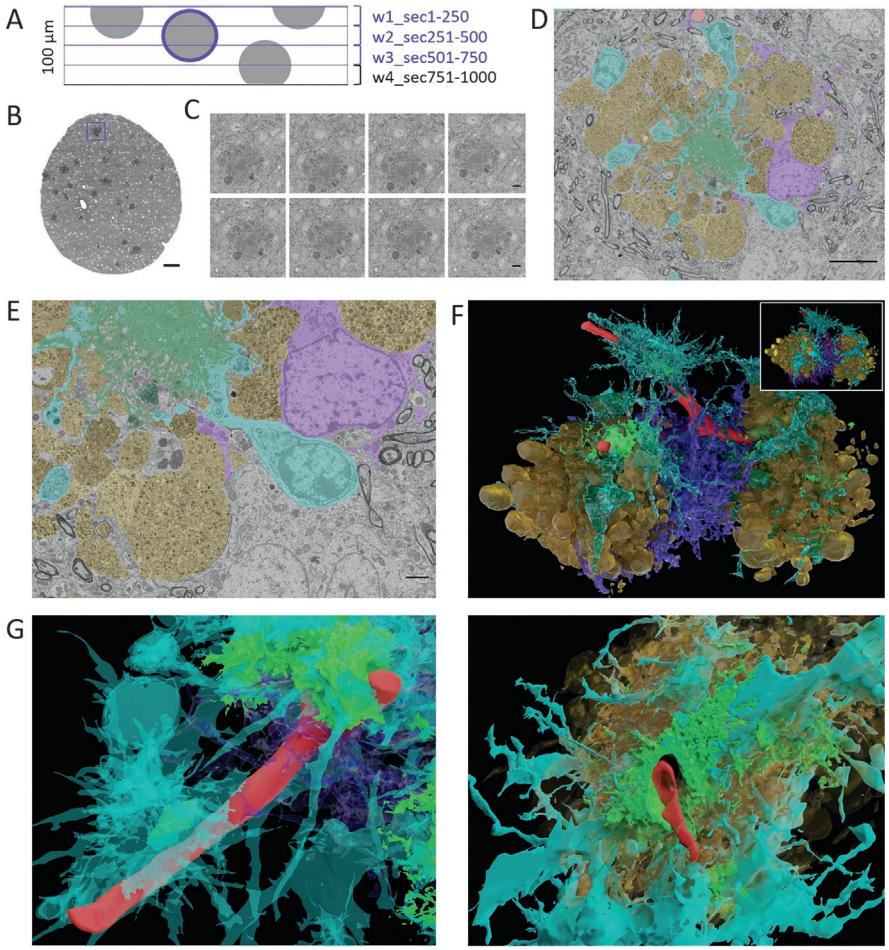

FIG. 8

ATUM acquisition of an AD plaque. AD mouse model APP/PS1, 6 months. (A) Schematic drawing of a vibratome cross-section of an AD mouse cortex with plaques (dark, round area). Only some plaques (blue border) of 50–80 µm diameter are fully contained within the section (thickness 100 µm) (top). After embedding, sectioning this tissue into 100 nm thick sections results in 1000 sections that are mounted onto four wafers. All wafers are screened for complete plaques. Only the first three wafers contain the plaque of interest and are needed for high resolution imaging (bottom). (B) SEM medium resolution ($200 \times 200 \times 1000$ nm) sufficient to identify plaques. The selected plaque (box) is selected for high-resolution imaging. Scale bar 100 µm. (C) Registration of high-resolution images of plaques on consecutive 100 nm thick sections before (top) and after (bottom) alignment. Scale bar 10 µm. (D) Segmentation of this plaque highlighting microglia (cyan), astrocytes (violet), blood vessel lumen (red), dystrophic neurites (orange) and amyloid core (green) using VAST 1.4.1. Scale bars 5 µm (left), 2 µm (right). (E) Three-dimensional reconstruction of the objects shown in (D) as shown in VAST and after rendering in Blender (F).

(Fig. 8B and C). In order to visualize a plaque and interacting cells, we performed a complete reconstruction (Fig. 8E and F). A 100 µm thick coronal cortical vibratome section was dissected, yielding a $1.5 \times 2 \times 0.1$ mm piece of tissue containing several plaques (Fig. 8A), which we stained using the "Ellisman protocol" (Deerinck et al., 2010). As we were primarily interested in contacts between microglial cells and plaque-associated structures, we opted for an ATUM tissue library of 100 nm ultrathin sections. We cut approximately 1000 sections and mounted them on four silicon wafers. Plaque regions were visible in a screening run acquiring the entire tissue area at $200 \times 200 \times 2000$ nm resolution (every 10th section) on all wafers (time: 2 d) (Fig. 8B). We selected a plaque that was fully contained within the tissue thickness corresponding to three wafers (Fig. 8A) and imaged it at high-resolution ($10 \times 10 \times 100$ nm) using Maps 3 as described. The tiles were stitched and the three data stacks aligned in TrakEM2 (Fig. 8C). Microglia (cyan), β-amyloid (green) and dystrophic neurites (orange), as well as the blood vessel lumen (red) were segmented in VAST (Berger et al., 2018) and rendered in Blender (Fig. 8D). In addition, sites of microglial contact with dystrophic neurites and the core were acquired as single two-dimensional images at 4×4 nm resolution (Fig. 8D). The tissue library approach enables screening for the (rare) target structure and enables complete reconstruction in order to obtain both, a three-dimensional insight, as well as high resolution images of target sites (Fig. 8E and F).

In a second example, we show that ATUM can be applied for the correlated ultrastructural reconstruction of a cortical spine in a cortical neuroinflammatory lesion, previously monitored and selected by 2-photon microscopy. Fluorescent imaging of a mouse with a genetically encoded calcium indicator Twitch2b expressed in neurons was performed through a cranial window. A dendrite with a specific spine with an abnormal calcium level was selected in this data set (Fig. 9D and E). After live imaging, the mouse was perfused, external landmarks were introduced at the surface and at the site of the selected spine using high laser power. This Near Infrared Branding (NIRB) (Bishop et al., 2011) technique introduces fluorescent landmarks that are visible as discrete sites of destroyed tissue in the ultrastructure and help to relocate the structure of interest in axial and lateral dimensions (Fig. 9D and E). The tissue was dissected around the superficial NIRB marks resulting in a $1.5 \times 1.5 \times 1$ mm block and embedded using the "Hua protocol" (Hua et al., 2015). We collected 50 nm thin sections on tape in order to capture the spine of interest at one of the highest axial resolutions that ATUM can provide. Collection was started at the very superficial cortical layers and sections were assembled on six wafers (Fig. 9A). The tissue was first imaged at low resolution ($0.2 \times 0.2 \times 2.5$ µm; every 50th section) to screen for the NIRB marks and further endogenous marks like blood vessels (Fig. 9A). Comparison of this screening data revealed that the spine of interest was located on wafers #3 or #4, which were in turn reimaged at medium resolution ($20 \times 20 \times 100$ nm; every 2nd section) (Fig. 9B). This second screening data set was smaller than the whole section as the coarse xy-orientation was already set in the low-resolution stack. Segmentation of several dendrites (Fig. 9E) helped to exclude false negative neurites and finally led to the relocation of the dendrite with the spine of interest that was imaged at $4 \times 4 \times 50$ nm resolution (Fig. 9E and F).

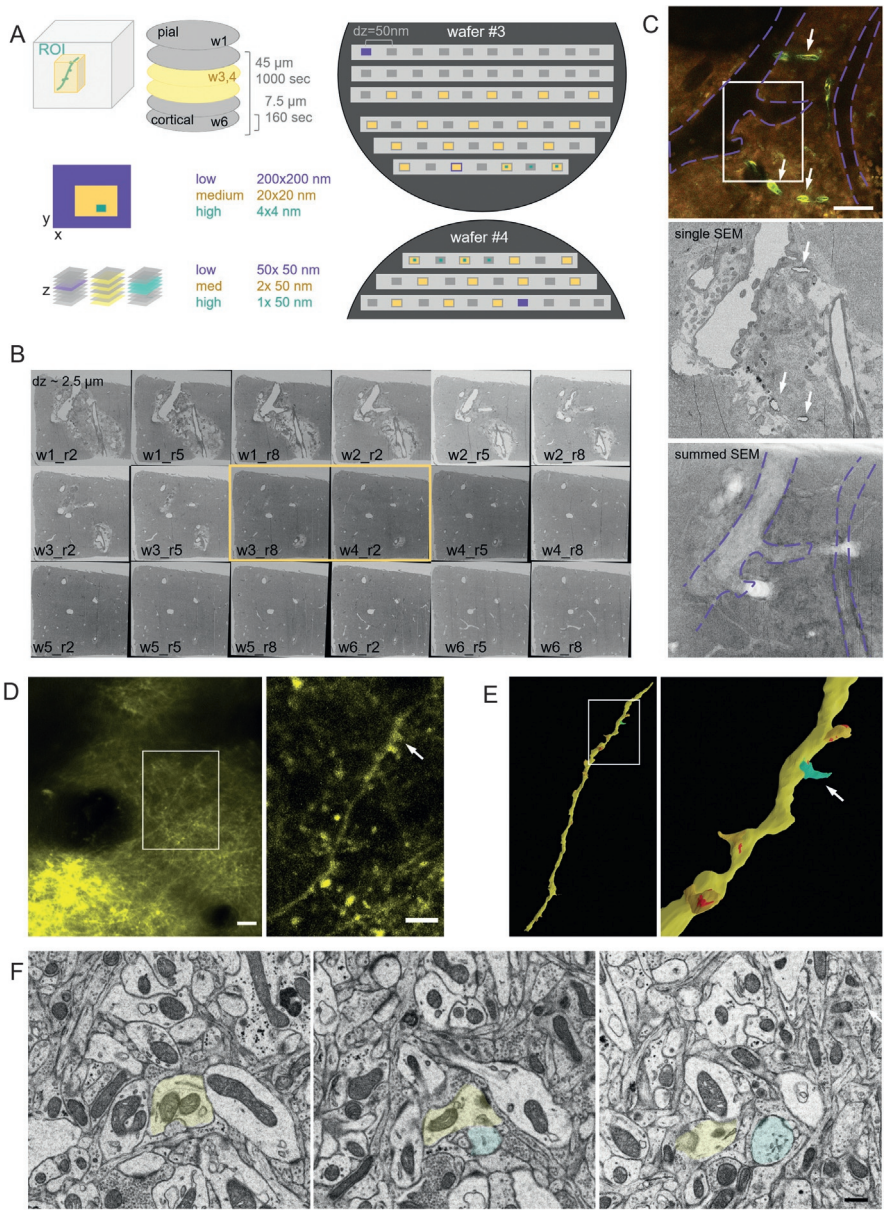

FIG. 9

Correlation of a single spine in mouse cortex using NIRB and ATUM. (A) Relocation strategy. 1000 sections were cut at 50 nm thickness and collected onto plastic tape by ATUM. Six wafers were mounted with 9 strips each. Low resolution (200 × 200 × 2500 nm) imaging was used for coarse registration, medium resolution (50 × 50 × 200 nm) imaging of every other section for fine correlation of the dendrite and high resolution (4 × 4 × 50 nm) imaging for

(Continued)

7 Limitations

The ATUM-SEM method is limited in axial resolution like all other microtomy-based vEM methods, including SBF-SEM. For conventional ATUM-SEM it is especially important to decide for a suitable tissue orientation in order to account for the anisotropic lateral ($>1 \times 1$ nm) vs axial (>30–50 nm) resolution. The anisotropic nature of the ATUM technique is especially challenging for subcellular structures like mitochondria. While a mitochondrium (0.5×5 μm) captured longitudinally would be visible on ~10 (50 nm thick) sections, a cross-sectioned one would span over ~100 sections with more information loss between the sections. In CLEM, a cell of interest can be relocated with high precision but its organellar distribution and orientation is unknown prior to ultrastructural analysis. Others and we have circumvented this drawback by combining semithick sectioning and collection with targeted FIB-SEM imaging (Baena et al., 2019; Hayworth et al., 2015; Kislinger et al., 2020b).

Serial sectioning procedures are sensitive toward disturbances and thus need to be tightly controlled. Any rotation, stretching, compression, uneven section thickness or folding of the tissue will have a major impact on the following steps, including mapping, imaging and image analysis (Fig. 10). This is the major drawback of collection-based vs more automatized block face techniques. The generation of tissue libraries and the modular nature of ATUM and AT comes with challenges in automation. Any disturbances during sectioning or contamination during mounting (Fig. 10D) can lead to imperfect alignment and loss of ultrastructural information.

Another big conundrum in serial sectioning and collection approaches is the discrepancy between the sample preparation requirements for serial sectioning vs imaging. High heavy metal load is needed for detection, especially for repetitive imaging of the same region of interest at high resolution. However, serial sectioning of *en bloc* stained samples can be difficult and lead to fold formation (Fig. 10C).

Compared to solid support AT or MagC (Templier, 2019), the section density per area of sections on tape is lower (Fig. 11). Consequently, this increases the number of sample (wafer) insertions and time-consuming mapping procedures. Moreover, the

FIG. 9—Cont'd visualization of the spine of interest as shown in (E). (B) Wafer overview mapping for relocation of the region of interest. SEM micrographs of wafers w 1–6, plastic strip rows r 2, 5, 8 are shown. (C) 2-Photon (upper; Twitch2b-YFP, yellow), single SEM (middle) and summed SEM (wafer 1–6, 18 images) (bottom) images from the same region. Vasculature (blue) and NIRB marks (white arrows) are fiducials that guide the relocation of the approximate region around the spine of interest. Scale bar 50 μm (D) 2-Photon (Twitch2b-YFP, yellow) overview (inset in (C) (scale bar 10 μm) and dendrite of interest (middle, z projection of 20 images covering 20 μm in thickness, scale bar 5 μm). (E) 3D model (covers 250 sections, 12.5 μm) reconstructed from the EM images. Dendrite (yellow), spine (orange), postsynaptic density (PSD, red), spine of interest (green, arrow). Scale bar 5 μm (F) High resolution electron micrographs of the spine of interest. Dendrite (yellow), spine of interest (green), PSD (red arrow) Scale bar 500 nm.

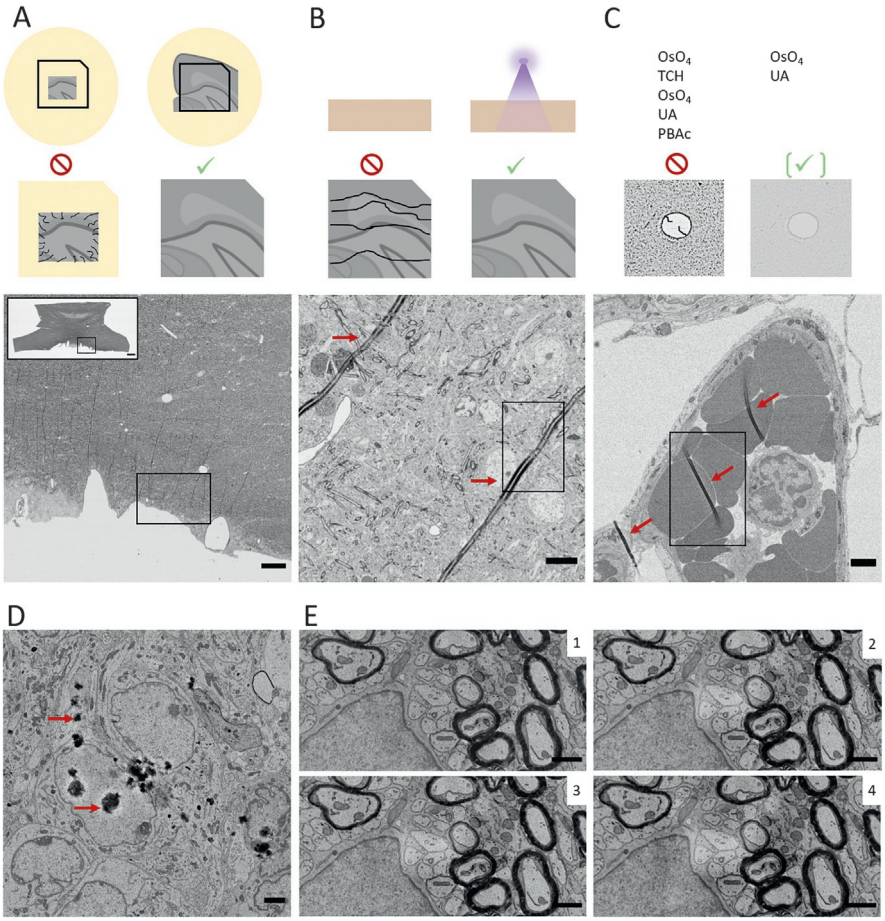

FIG. 10

Limitations of image and registration quality due to folds, impurities and beam damage. (A–C) Fold problems illustrated by schematics (top) and example BSD images (bottom). (A)The tissue to resin (yellow) ratio needs to be high to avoid folds at the interface. Top view onto tissue blocks in resin (top). The right option with bigger tissue is preferred as the tissue-resin interface is avoided. Scale bar 50 μm. (B) Tape (brown) plasma treatment (violet) reduces collection folds. Scale bar 2 μm. (C). A lower heavy metal load avoids microscale folds in tissue structures like the empty (resin-filled) blood vessel lumen. (D) BSD image with dirt on the section which can occur through diverse handling steps. Folds and dirt are highlighted (red arrows). Scale bar 2 μm. (E) BSD images of the same region on a mouse optic nerve ultrathin (50 nm) section after repetitive imaging (once (1, twice (2), three (3) or four (4) times). The central autofocus region shows increasing beam damage. Scale bar 1 μm.

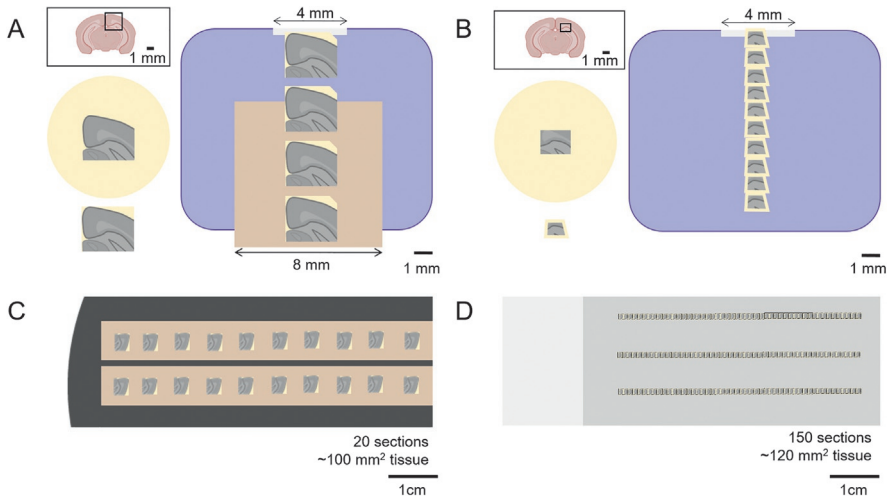

FIG. 11

Comparison of scales in ATUM vs solid support AT. Schematic in scale drawings of samples at different steps during the ATUM (A, C) and AT (B, D) workflows. (A, B) Insets show a coronal cross section with the dissected tissue boxed (top left). Top view onto the tissue (gray) in the resin block (yellow) (middle left) and a representative section after trimming (lower left). Top view on diamond knife (right, blue) with the length of the knife edge (4 mm) and the tape (brown) width (8 mm) indicated. (A) Single bigger (2×2.5 mm) sections (B) or a ribbon of smaller (1×0.8 mm) trapezoid sections (B) are collected, respectively. (C) A cutout of an assembled silicon wafer with two strips that corresponds to the size of a glass slide (D) is shown. While the ATUM wafer cutout carries 20 bigger sections, the AT glass slide is covered by 150 sections. While the section number and therefore the covered tissue thickness are higher in AT (2 vs 15 μm), the tissue area is similar (100 vs 120 mm^2).

sample spread over a huge area leads to variations in focal heights, which has to be taken into account for autofocusing. Adding to this, the sections are not collected directly onto support material (like AT glass, MagC silicon) but require two levels of tape (CNT/ccKapton, carbon adhesive) which increases the variability of working distance between different sections or strips (Fig. 7K).

Apart from technical challenges, one of the problems of the ATUM method is the lack of a reliable commercial supply of conductive plastic tape. CNT and non-coated Kapton are tapes provided by industry partners, while ccKapton is not sold by any company despite its advantages. One way to circumvent this supply problem is to work with non-conductive tape and carbon-coat after wafer assembly. Since this introduces a carbon layer on top of the sections, SE-detection is not accessible anymore and requires BSD detection.

8 Advantages

Compared to destructive block face methods, ATUM and solid support AT separate the sectioning from the serial acquisition procedure. This modularity enables flexible protocol execution at varying time points and even by different scientists at distinct sites. Parallel implementation is a great advantage, especially in facilities that run many projects in parallel. Moreover, serial section collection preserves precious samples, which can consequently be stored on wafers as a tissue library. The physical storage of tissue sections enables post-treatments, such as heavy metal or antibody staining. Importantly, the collection can be reinspected with immutable axial resolution but at different lateral resolution levels. Autofocusing can, however lead to local beam damage on repetitively imaged regions (Fig. 10E). Low-resolution overview imaging is especially helpful to reorient within a tissue that has previously been imaged by light microscopy. Characteristic structures in the tens hundreds of µm scale surrounding the ROI like blood vessels can be visualized in both modalities. Hierarchical imaging enables the inspection of these fiducial objects within a large area thereby guiding the targeting process for the relocation of the ROI that, in turn, is reimaged at high resolution. While this enlarged search area and volume is crucial for CLEM workflows, any kind of ultrastructural analysis highly benefits from preservation of environmental information.

Solid support AT and ATUM share many of the unique advantages of section preservation compared to destructive vEM techniques. As the generation of section ribbons needed for solid support AT gets more difficult with bigger block faces, serial single sectioning as required for ATUM-SEM is superior for larger sections (Fig. 11). Hence, ATUM-SEM provides more flexible screening areas which is beneficial for vEM in general and targeted or correlated vEM more specifically (Shibata et al., 2019). From our experience, section collection on tape is easier to learn than ribbon sectioning for solid support AT. In addition, different lateral resolution schemes ranging from 30 to 500 nm (with ATUM-FIB even up to 5 µm (Kislinger et al., 2020b) can be applied which broadens the scaling options to anatomical reconstructions of larger tissue structures (Terasaki et al., 2020). Taken together, AT techniques in general, and ATUM-SEM more specifically, provide an enormous scaling and handling flexibility, which facilitates the three-dimensional rendering of differently sized structures and the screening for specific target objects.

Acknowledgments

This work was supported by DFG under Germany's Excellence Strategy within the framework of the Munich Cluster for Systems Neurology (EXC 2145 SyNergy, ID 390857198) and the TRR 274/1 2020, 408885537 (project Z01). We thank Mark Terasaki and Richard Schalek for valuable scientific and technical advice, as well as Christian Haass for providing APP/PS1 brain samples.

References

Baena, V., & Terasaki, M. (2019). Three-dimensional organization of transzonal projections and other cytoplasmic extensions in the mouse ovarian follicle. *Scientific Reports*, *9*(1), 1262.

Baena, V., et al. (2019). Serial-section electron microscopy using automated tape-collecting ultramicrotome (ATUM). *Methods in Cell Biology*, *152*, 41–67.

Bang, B. H., & Bang, F. B. (1957). Graphic reconstruction of the third dimension from serial electron microphotographs. *Journal of Ultrastructure Research*, *1*(2), 138–139.

Berger, D. R., Sebastian Seung, H., & Lichtman, J. W. (2018). VAST (volume annotation and segmentation tool): Efficient manual and semi-automatic labeling of large 3D image stacks. *Frontiers in Neural Circuits*, *12*, 88.

Bishop, D., et al. (2011). Near-infrared branding efficiently correlates light and electron microscopy. *Nature Methods*, *8*(7), 568–570.

Brito, A. (2018). *Blender Quick Start Guide: 3D Modeling, Animation, and Render with Eevee in Blender 2.8*. Packt Publishing.

Burel, A., et al. (2018). A targeted 3D EM and correlative microscopy method using SEM array tomography. *Development*, *145*(12), dev160879.

Cardona, A., et al. (2012). TrakEM2 software for neural circuit reconstruction. *PLoS One*, *7*(6), e38011.

Collman, F., et al. (2015). Mapping synapses by conjugate light-electron array tomography. *The Journal of Neuroscience*, *35*(14), 5792–5807.

De Rosier, D. J., & Klug, A. (1968). Reconstruction of three dimensional structures from electron micrographs. *Nature*, *217*(5124), 130–134.

Deerinck, T. J., et al. (2010). NCMIR methods for 3D EM: A new protocol for preparation of biological specimens for serial block face scanning electron microscopy. *National Center for Microscopy and Imaging Research*, 6–8.

Denk, W., & Horstmann, H. (2004). Serial block-face scanning electron microscopy to reconstruct three-dimensional tissue nanostructure. *PLoS Biology*, *2*(11), e329.

Djannatian, M., et al. (2019). Two adhesive systems cooperatively regulate axon ensheathment and myelin growth in the CNS. *Nature Communications*, *10*(1), 4794.

Eberle, A. L., & Zeidler, D. (2018). Multi-beam scanning electron microscopy for high-throughput imaging in connectomics research. *Frontiers in Neuroanatomy*, *12*(112).

Fang, T., et al. (2018). Nanobody immunostaining for correlated light and electron microscopy with preservation of ultrastructure. *Nature Methods*, *15*(12), 1029–1032.

Gay, H., & Anderson, T. F. (1954). Serial sections for electron microscopy. *Science*, *120*(3130), 1071–1073.

Genoud, C., et al. (2018). Fast homogeneous En bloc staining of large tissue samples for volume Electron microscopy. *Frontiers in Neuroanatomy*, *12*(76).

Harris, K. M., et al. (2006). Uniform serial sectioning for transmission electron microscopy. *The Journal of Neuroscience*, *26*(47), 12101–12103.

Hayworth, K. J., et al. (2014). Imaging ATUM ultrathin section libraries with WaferMapper: A multi-scale approach to EM reconstruction of neural circuits. *Frontiers in Neural Circuits*, *8*, 68.

Hayworth, K. J., et al. (2015). Ultrastructurally smooth thick partitioning and volume stitching for large-scale connectomics. *Nature Methods*, *12*(4), 319–322.

Herwerth, M., et al. (2022). A new form of axonal pathology in a spinal model of neuromyelitis optica. *Brain*.

Hildebrand, D. G. C., et al. (2017). Whole-brain serial-section electron microscopy in larval zebrafish. *Nature*, *545*(7654), 345–349.

Hirabayashi, Y., Tapia, J. C., & Polleux, F. (2018). Correlated light-serial scanning electron microscopy (CoLSSEM) for ultrastructural visualization of single neurons in vivo. *Scientific Reports*, *8*(1), 14491.

Hua, Y., Laserstein, P., & Helmstaedter, M. (2015). Large-volume En-bloc staining for electron microscopy-based connectomics. *Nature Communications*, *6*(1), 7923.

Kamasawa, N., et al. (2015). Correlative ultrastructural analysis of functionally modulated synapses using automatic tape-collecting ultramicrotome-SEM array tomography. *Microscopy and Microanalysis*, *21*(S3), 1271–1272.

Kasthuri, N., et al. (2015). Saturated reconstruction of a volume of neocortex. *Cell*, *162*(3), 648–661.

Kislinger, G., et al. (2020a). ATUM-FIB microscopy for targeting and multiscale imaging of rare events in mouse cortex. *STAR Protocols*, *1*(3), 100232.

Kislinger, G., et al. (2020b). Multiscale ATUM-FIB microscopy enables targeted ultrastructural analysis at isotropic resolution. *iScience*, *23*(7). 101290.

Kornfeld, J., & Denk, W. (2018). Progress and remaining challenges in high-throughput volume electron microscopy. *Current Opinion in Neurobiology*, *50*, 261–267.

Kubota, Y., et al. (2018). A carbon nanotube tape for serial-section electron microscopy of brain ultrastructure. *Nature Communications*, *9*(1), 437.

Li, X., et al. (2017). Large scale three-dimensional reconstruction of an entire Caenorhabditis elegans larva using AutoCUTS-SEM. *Journal of Structural Biology*, *200*(2), 87–96.

Liesche-Starnecker, F., et al. (2022). Hemorrhagic lesion with detection of infected endothelial cells in human bornavirus encephalitis. *Acta Neuropathologica*, *144*(2), 377–379.

Luckner, M., & Wanner, G. (2018). Precise and economic FIB/SEM for CLEM: With 2 nm voxels through mitosis. *Histochemistry and Cell Biology*, *150*(2), 149–170.

Micheva, K. D., & Phend, K. D. (2018). Conjugate immunofluorescence—SEM Array tomography for studying mammalian synapses and axons. In E. Hanssen (Ed.), *Cellular imaging: Electron tomography and related techniques* (pp. 149–182). Cham: Springer International Publishing.

Micheva, K. D., & Smith, S. J. (2007). Array tomography: A new tool for imaging the molecular architecture and ultrastructure of neural circuits. *Neuron*, *55*(1), 25–36.

Mikula, S., & Denk, W. (2015). High-resolution whole-brain staining for electron microscopic circuit reconstruction. *Nature Methods*, *12*(6), 541–546.

Mikuni, T., et al. (2016). High-throughput, high-resolution mapping of protein localization in mammalian brain by in vivo genome editing. *Cell*, *165*(7), 1803–1817.

Mondo, E., et al. (2020). A developmental analysis of Juxtavascular microglia dynamics and interactions with the vasculature. *The Journal of Neuroscience*, *40*(34), 6503–6521.

Morales, A. G., et al. (2016). Micro-CT scouting for transmission electron microscopy of human tissue specimens. *Journal of Microscopy*, *263*(1), 113–117.

Morgan, J. L., et al. (2016). The fuzzy logic of network connectivity in mouse visual thalamus. *Cell*, *165*(1), 192–206.

Norris, R. P., & Terasaki, M. (2021). Gap junction internalization and processing in vivo: A 3D immuno-electron microscopy study. *Journal of Cell Science*, *134*(1).

Parlanti, P., et al. (2017). Size and specimen-dependent strategy for x-ray micro-ct and tem correlative analysis of nervous system samples. *Scientific Reports*, *7*(1), 2858.

Peddie, C. J., et al. (2022). Volume electron microscopy. *Nature Reviews Methods Primers*, *2*(1), 51.

Radde, R., et al. (2006). Aβ42-driven cerebral amyloidosis in transgenic mice reveals early and robust pathology. *EMBO Reports*, *7*(9), 940–946.

Rawson, S. D., et al. (2020). X-ray computed tomography in life sciences. *BMC Biology*, *18*(1), 21.

Schalek, R., et al. (2012). ATUM-based SEM for high-speed large-volume biological reconstructions. *Microscopy and Microanalysis*, *18*, 572–573.

Schifferer, M., et al. (2021). Niwaki instead of random forests: Targeted serial sectioning scanning electron microscopy with reimaging capabilities for exploring central nervous system cell biology and pathology. *Frontiers in Neuroanatomy*, *15*, 732506.

Schindelin, J., et al. (2012). Fiji: An open-source platform for biological-image analysis. *Nature Methods*, *9*(7), 676–682.

Shapson-Coe, A., et al. (2021). A connectomic study of a petascale fragment of human cerebral cortex. *bioRxiv*. 2021.05.29.446289.

Shibata, S., et al. (2019). Large-area fluorescence and Electron microscopic correlative imaging with multibeam scanning electron microscopy. *Frontiers in Neural Circuits*, *13*, 29.

Snaidero, N., et al. (2020). Myelin replacement triggered by single-cell demyelination in mouse cortex. *Nature Communications*, *11*(1), 4901.

Sun, Y., et al. (2020). Correlative ultrastructural analysis of functionally modulated synapses using automated tape-collecting Ultramicrotome and SEM scanning electron microscopy (SEM) array tomography. In I. Wacker, E. Hummel, S. Burgold, & R. Schröder (Eds.), *Volume microscopy: Multiscale imaging with photons, electrons, and ions* (pp. 121–149). New York, NY: Springer US.

Tapia, J. C., et al. (2012). High-contrast En bloc staining of neuronal tissue for field emission scanning electron microscopy. *Nature Protocols*, *7*(2), 193–206.

Templier, T. (2019). MagC, magnetic collection of ultrathin sections for volumetric correlative light and electron microscopy. *eLife*, *8*, e45696.

Terasaki, M., Brunson, J. C., & Sardi, J. (2020). Analysis of the three dimensional structure of the kidney glomerulus capillary network. *Scientific Reports*, *10*(1), 20334.

Terasaki, M., et al. (2013). Stacked endoplasmic reticulum sheets are connected by Helicoidal membrane motifs. *Cell*, *154*(2), 285–296.

Thestrup, T., et al. (2014). Optimized ratiometric calcium sensors for functional in vivo imaging of neurons and T lymphocytes. *Nature Methods*, *11*(2), 175–182.

Thomas, C. I., et al. (2019). Presynaptic mitochondria volume and abundance increase during development of a high-Fidelity synapse. *The Journal of Neuroscience*, *39*(41), 7994–8012.

Tomassy, G. S., et al. (2014). Distinct profiles of myelin distribution along single axons of pyramidal neurons in the neocortex. *Science*, *344*(6181), 319–324.

Wacker, I., & Schroeder, R. R. (2013). Array tomography. *Journal of Microscopy*, *252*(2), 93–99.

Wacker, I. U., et al. (2018). Multimodal hierarchical imaging of serial sections for finding specific cellular targets within large volumes. *JoVE*, *133*, e57059.

Wanner, A. A., & Vishwanathan, A. (2018). Methods for mapping neuronal activity to synaptic connectivity: Lessons from larval zebrafish. *Frontiers in Neural Circuits*, *12*.

White, J. G., et al. (1986). The structure of the nervous system of the nematode Caenorhabditis elegans. *Philosophical Transactions of the Royal Society of London. Series B, Biological Sciences*, *314*(1165), 1–340.

Witte, M. E., et al. (2019). Calcium influx through plasma-membrane nanoruptures drives axon degeneration in a model of multiple sclerosis. *Neuron*, *101*(4), 615–624.e5.

Yan, H., Voorhees, P. W., & Xin, H. L. (2020). Nanoscale X-ray and electron tomography. *MRS Bulletin*, *45*(4), 264–271.